Dimethyl Peroxide Radical Cation: A New Theoretical and Experimental Approach to the $C_2H_6O_2^{\bullet+}$ Potential Energy Surface

Christoph A. Schalley, Andreas Fiedler, Georg Hornung, Ralf Wesendrup, Detlef Schröder, and Helmut Schwarz*

Abstract: The structure and the unimolecular fragmentations of the metastable dimethyl peroxide radical cation have been investigated by mass spectrometric and isotopic labeling methods as well as high-level ab initio calculations. In line with the theoretical results, neutralization–reionization and charge reversal experiments suggest that ionized dimethyl peroxide bears a $CH_3OOCH_3^{\bullet+}$ connectivity. In the cation the O–O bond dissociation energy is larger than that of the neutral counterpart; in contrast, the C–O bond strength is slightly and that of the C–H bond significantly reduced upon ionization. These energetic changes upon one-electron oxidation of CH_3OOCH_3 are also reflected in the NR and CR mass spectra of $CH_3OOCH_3^{\bullet+}$. Further, for metastable $CH_3OOCH_3^{\bullet+}$ two major fragmentation pathways are observed: 1) Loss of a hydrogen atom by cleavage of a C–H bond is associated with a skeletal reorganization, which gives rise to a proton-bound formaldehyde dimer. 2) The expulsion of a $CH_3O^{\bullet}$ radical leads to protonated formaldehyde in a surprisingly specific double hydrogen transfer involving a $[CH_3OH/CH_2O]^{\bullet+}$ ion/dipole complex as central intermediate; this complex also accounts for other minor fragmentation channels. The structures of intermediates and transition states are calculated with the BECKE3LYP density-functional method employing a 6-311++G** basis.

Keywords
ab initio calculations · dimethyl peroxide · mass spectrometry · peroxides · radical ions

Introduction

Mass spectrometry and ab initio calculations are complementary tools that are ideally suited for the investigation of gas-phase structures and unimolecular fragmentation patterns of small ions and neutrals.[1] The $[C_2,H_6,O_2]^{\bullet+}$ potential-energy surface has been examined repeatedly in combined mass spectrometric and theoretical studies, and the ethylene glycol radical cation $\mathbf{3}^{\bullet+}$ was often used as a starting point.[2] Several distonic ions,[2b] hydrogen-bridged cations,[2a, c] and ion/dipole complexes[2d, 3] have been proposed as intermediates in the fragmentation of $\mathbf{3}^{\bullet+}$, and a complex reaction mechanism involving dipole-catalyzed proton shifts and charge transfer processes has been suggested in order to explain the experimental findings.[2e, 4] Surprisingly, other entries to the $[C_2,H_6,O_2]^{\bullet+}$ potential-energy surface have hardly been used so far. Burgers et al.[2a] reported that the metastable radical cations of ethyl hydroperoxide $\mathbf{2}^{\bullet+}$ and dimethyl peroxide $\mathbf{1}^{\bullet+}$ undergo fragmentations that are entirely different from those of $\mathbf{3}^{\bullet+}$, such that the rearrangements $\mathbf{1}^{\bullet+} \rightarrow \mathbf{3}^{\bullet+}$ and $\mathbf{2}^{\bullet+} \rightarrow \mathbf{3}^{\bullet+}$ can be excluded. More detailed investigation of these peroxides appear to be necessary in order to unravel additional parts of the $[C_2,H_6,O_2]^{\bullet+}$ potential-energy surface.

As far as the mass spectrometry of small dialkyl peroxides is concerned, detailed investigations are scarce.[5] For dimethyl peroxide the EI mass spectrum and metastable decompositions have been reported,[6] and protonated **1** and **2** have been struc-

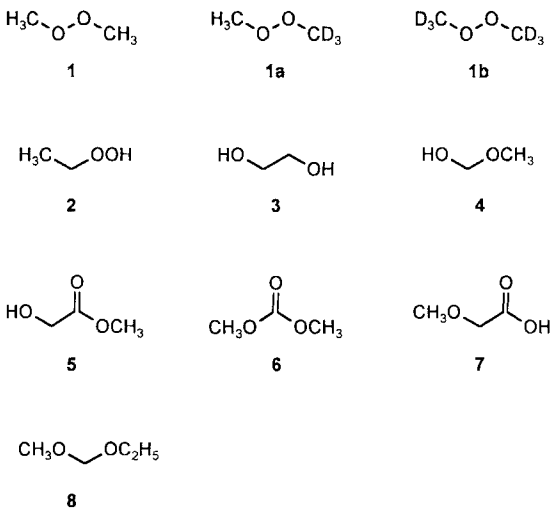

[*] H. Schwarz, C. A. Schalley, G. Hornung, R. Wesendrup, D. Schröder
Institut für Organische Chemie der Technischen Universität Berlin
Straße des 17. Juni 135, D-10623 Berlin (Germany)
Telefax: Int. code +(30)314-21102
e-mail: schw0531@zrzsp5.chem.tu-berlin.de
A. Fiedler
Institute for Molecular Sciences, Myodaiji, 444 Okasaki (Japan)

0947-6539/97/0304-0626 $ 17.50+.50/0

turally characterized by mass spectrometric and theoretical methods,[7] but in none of these studies has isotopic labeling been carried out. Recently, a more thorough investigation of the unimolecular fragmentations of the methyl nitrite radical cation,[8] which bears a weak N–O bond similar to the O–O bond in $CH_3OOCH_3^{\bullet+}$, revealed a quite complex fragmentation pattern. In this respect, it seems to be particularly interesting to understand how the presence of O–O bonds bias the reactivity pattern in the unimolecular decay of peroxide radical cations.

In this article, we present a detailed mass spectrometric and theoretical study of the dimethyl peroxide radical cation and its unimolecular decompositions. For comparison, compounds **2**–**8** were included in this study, because these are either structural isomers of CH_3OOCH_3 or represent promising precursors for the generation of other $[C_2,H_6,O_2]^{\bullet+}$ ions through loss of carbon monoxide or ethene, respectively, from their ionized analogues.

Experimental Section

The experiments were performed with a modified VG ZAB/HF/AMD four-sector mass spectrometer of BEBE configuration (B stands for magnetic and E for electric sector), which has been described previously.[9] Briefly, the substrates were ionized by a beam of electrons having 70 eV kinetic energy in an EI ion source. To avoid peroxide decomposition, a metal-free Teflon/glass inlet system was used for the introduction of the peroxides into the ion source.[10] The ions were accelerated to 8 keV translational energy and mass-selected by means of B(1)/E(1) at a resolution of $m/\Delta m \approx 3000-4000$; isobaric impurities were not observed. Unimolecular fragmentations of metastable ions (MI) occurring in the field-free region preceding B(2) were recorded by scanning this sector. For collisional activation (CA), B(1)/E(1) mass-selected ions were collided with helium (80% transmission, T). The error of the relative intensities in MS/MS experiments does not exceed ±5%.

MS/MS/MS experiments[11] were performed by selecting the fragment ions of interest by means of B(2), and the collision-induced fragmentations (He, 80% T) occurring in the subsequent field-free region were monitored by scanning E(2); these experiments will be referred to as MI/CA spectra. The sensitivity in MS/MS/MS experiments is less than that of the MS/MS studies, and the error is estimated at ±15%. Consecutive fragmentations can be studied by MI/MI experiments, if the second decomposition is not too fast and occurs in the μsec time-window of these experiments.[12] Faster processes (nsec timescale) can be studied by applying the ion retardation method,[13] in which the beam of metastable ions is influenced by an electric potential on a collision gas cell (no collision gas leaked in). Direct fragmentation reactions then lead to two different signals in the MI mass spectrum, one for the ions fragmenting outside, the other representing ions decomposing inside the cell. In such a set-up, consecutive processes give rise to additional signals, provided one neutral is lost outside and the other inside the cell. From the signal shifts observed in this experiment, one can deduce, which neutrals have been formed during the decomposition. For instrumental reasons, the retardation experiments were carried out in the field-free region between B(1) and E(1).

For neutralization–reionization (NR) experiments,[14] the cations ($^+NR^+$)[14d,15] were neutralized by high-energy collisions with xenon (80% T) in the first of two differentially pumped collision cells located in the field-free region between E(1) and B(2). Unreacted ions were deflected away from the beam of neutral species by applying a voltage of 1 kV on a deflector electrode located between the two collision chambers. Subsequent reionization to cations occurred in a second cell by collisions with oxygen (80% T). The resulting mass spectra were recorded by scanning B(2). For collisional activation of survivor ions ($^+NR^+$/CA), these ions were selected with B(2) and collided with helium (80% T) in the subsequent field-free region, and the ionic products were monitored using E(2).

Collisionally induced dissociative ionization (CIDI) mass spectra[16] were performed in the field-free region between E(1) and B(2) by deflecting away all ions from the beam of neutrals generated upon unimolecular decay, and subsequent ionization of the remaining neutrals by high energy collisions with oxygen. Owing to low intensities a relatively high O_2 pressure was applied (60% T). Differential pumping and use of a flight path of ca. 80 cm ensured the absence of $^+NR^+$ processes in the CIDI mass spectra, as indicated by the absence of survivor ions, which represent the base peak in the $^+NR^+$ mass spectra of $\mathbf{1}^{\bullet+}$ (see below).

Charge reversal mass spectra of cationic $\mathbf{1}^{\bullet+}$ to anionic fragments ($^+CR^-$)[9c,17] were obtained by colliding the ion beam with benzene (70% T). Owing to low signal intensities these experiments were carried out in the field-free region between B(1) and E(1). Analogously, $^+NR^-$ mass spectra were obtained in the same field-free region, by neutralizing the cations with Xe (80% T), deflecting away the unreacted ions from the beam, and reionizing the neutral species to anions with benzene (70% T).

Kinetic energy release values, $T_{0.5}$, associated with the fragmentations of B(1) mass-selected $\mathbf{1}^{\bullet+}$ were estimated from peak half-height widths[18] at an energy spread of the parent ions of ca. 2 V. All spectra were accumulated and processed on-line with the AMD-Intectra data system; 5 to 30 scans were averaged to improve the signal-to-noise ratio.

In additional experiments, the reaction of $CH_2O^{\bullet+}$ with CD_3OH was studied with a Spectrospin CMS 47X Fourier-transform ion cyclotron resonance (FT-ICR) mass spectrometer equipped with an external EI ion source.[19] In brief, $CH_2O^{\bullet+}$ ions were generated from formaldehyde by a beam of electrons (70 eV) and transferred by a system of electric potentials and lenses to the analyzer cell located within a superconducting magnet (7.05 T, Oxford Instruments). After thermalization by applying several argon pulses, $CH_2O^{\bullet+}$ was mass-selected using FERETS, a computer-controlled ion ejection protocol, which combines single-frequency ion ejection pulses with frequency sweeps to optimize ion isolation.[20] [D_3]methanol was admitted to the cell through a leak valve at a pressure of ca. 10^{-8} mbar. All functions of the instrument were controlled by a Bruker Aspect 3000 minicomputer.

Ethylene glycol, methyl 2-hydroxyacetate, dimethyl carbonate, and methoxyacetic acid (**3**, **5**–**7**) were used as purchased (Aldrich). Compounds **1** and **1b** were synthesized[21] by alkylation of hydrogen peroxide under basic conditions with [D_0]- and [D_6]dimethyl sulfate, respectively; **1a** was prepared from methyl hydroperoxide[22] by the same alkylation procedure using [D_6]-dimethyl sulfate (Acros, >99 atom% D). Ethyl hydroperoxide (**2**) was generated by treating the ethyl chloride Grignard reagent with oxygen and subsequent hydrolysis.[23,23] Ethoxymethoxymethane (**8**) was synthesized by treating sodium ethoxide with methoxymethyl chloride.[24,25] All compounds were purified by distillation and characterized by their ^1H NMR spectra[26] or EI mass spectra.[6] Note that dimethyl peroxide and ethyl hydroperoxide are hazardous substances and should be handled with appropriate precautions.[27] Therefore, peroxides were synthesized in small amounts (<0.5 g) and stored in a −20 °C refrigerator. As dimethyl peroxide may explode for no apparent reason, it was handeled as a pure substance only when cooled to at least −78 °C.

Computational Details: All calculations were carried out with the BECKE3LYP DFT/HF hybrid method as implemented in the GAUSSIAN 94[28] program using the Becke 3 parameter fit for atomization energies and the G2[29] set for the ionization energies of small molecules. In view of the large number of molecules and ions, which had to be calculated with an appropriately big basis set, this method was chosen, because it promised to be a rather cheap, but quite exact approach. The standard triple ζ split basis set (6-311 G)[30] was augmented by additional diffuse and polarization functions resulting in a 6-311++G** basis. This kind of basis set is necessary for a reasonable description of loosely bound complexes, such as H-bridged radical cations. Geometry optimizations were performed by using gradient procedures. Vibrational frequencies were calculated in order to characterize stationary points as minima or transition-state structures and to account for zero-point vibrational energy (ZPVE) corrections. ZPVE values are given unscaled, because the scaling factors are close to unity for the BECKE3LYP method.[31] It is expected that this method provides an accuracy of ca. ±5 kcal mol^{-1}.[32] This has been found also for several other peroxidic systems, such as H_2O_2[33] and CH_3OOH,[34] for which the BECKE3LYP energies were compared to G2 and CCSD(T)/TZ2P+f calculations. For radicals and radical cations, the s^2 values were close to 0.75, indicating that the contribution of quartet states is negligible. In order to determine the exact reaction pathway downhill, one of the central transition-state structures was investigated at the BECKE3LYP level of theory with the intrinsic reaction coordinate (IRC)[35] algorithm as introduced by Gonzalez and Schlegel;[36] for economic reasons, the IRC calculations were carried out using a 3-21 G*

Table 1. Mass differences (Δm in amu) observed in the CA mass spectra of isomeric $[C_2,H_6,O_2]^{\bullet+}$ cations [a,b].

Precursor		$-\Delta m =$	1	15	17	18	19	28	29	30	31	32	33	34	35	47	48
$CH_3OOCH_3^{\bullet+}$	$\mathbf{1}^{\bullet+}$		100 [c]	8	2				3	9	96 [c]	27 [c]	41	1		8	1
$CH_3CH_2OOH^{\bullet+}$	$\mathbf{2}^{\bullet+}$			15	100 [c]		13						44	4	6	2	
$HOCH_2CH_2OH^{\bullet+}$	$\mathbf{3}^{\bullet+}$		12	1		1	3	3	100 [c]	8	26	2	5			1	
$HOCH_2COOCH_3^+ - CO$	$[\mathbf{5}-CO]^{\bullet+}$		23 [c]	1	1	1	1	5	100 [c]	17	42	5	8			1	
$CH_3OCOOCH_3^+ - CO$	$[\mathbf{6}-CO]^{\bullet+}$		25 [c]	1	1	1	1	2	100 [c]	10	51	4	7			1	

[a] Intensities are given relative to the base peak = 100%. Some minor processes are omitted. [b] Part of these data have been published earlier by Burgers et al. [2a] and were remeasured here to ensure comparability. [c] These fragmentations are also observed in the MI mass spectra with more than 5% intensity relative to the sum of fragmentations.

basis set. Owing to the large amount of computer time necessary, we did not perform IRC calculations with the other transition-state structures, which are located energetically far below the internal energy contents of the ions formed from $\mathbf{1}^{\bullet+}$ (see below).

Results and Discussion

In the following sections we will first discuss the structure of $\mathbf{1}^{\bullet+}$, as far as conclusions can be drawn from a comparison of experiment and theory. Then, the metastable ion decompositions and the structural characterization of the resulting ionic products will be described. With the experimental results serving as a guideline, this section will be followed by a discussion of the calculated energetic and structural properties of central intermediates and transition-state structures. Finally, a mechanistic picture will evolve, which agrees well with the present and previous experimental results as well as thermochemical data.

The structure of the dimethyl peroxide radical cation: Four different experimental approaches were used in order to determine the connectivity of the $[C_2,H_6,O_2]^{\bullet+}$ species formed upon ionization of dimethyl peroxide.

First approach: If the MI and CA mass spectra of $\mathbf{1}^{\bullet+}$ differ clearly from those of other $[C_2,H_6,O_2]^{\bullet+}$ isomers, these structures can be ruled out for $\mathbf{1}^{\bullet+}$. Further, the possibility of a rearrangement of the major part of $\mathbf{1}^{\bullet+}$ to these isomers prior to dissociation can be discarded. However, from these experiments, the isomeric species cannot be ruled out as short-lived intermediates in the course of ion fragmentation of ionized **1**. Table 1 summarizes the CA mass spectra of different $[C_2,H_6,O_2]^{\bullet+}$ ions. It is obvious that the CA spectra of $\mathbf{2}^{\bullet+}$, $\mathbf{3}^{\bullet+}$, $[\mathbf{5}-CO]^{\bullet+}$, and $[\mathbf{6}-CO]^{\bullet+}$ are distinctly different from that of $\mathbf{1}^{\bullet+}$. While the loss of $H^{\bullet}$ ($\Delta m = 1$) corresponds to the base peak in the CA mass spectrum of $\mathbf{1}^{\bullet+}$, for $\mathbf{2}^{\bullet+}$ the expulsion of an $OH^{\bullet}$ ($\Delta m = 17$) radical is the most prominent process. The CA spectra of $\mathbf{3}^{\bullet+}$, $[\mathbf{5}-CO]^{\bullet+}$, and $[\mathbf{6}-CO]^{\bullet+}$ are dominated by the formation of $CH_3OH_2^+$ ions formed through the loss of neutral $HCO^{\bullet}$ radicals ($\Delta m = 29$). Finally, in the CA spectrum of $\mathbf{1}^{\bullet+}$, the peak corresponding to the formation of $[C,H_3,O]^+$ ($\Delta m = 31$) ions is found to be much more intense than in the spectra of the other isomers. The ion $\mathbf{3}^{\bullet+}$ has been reported[2b] to rearrange to the distonic ion $^{\bullet}OCH_2CH_2OH_2^+$, while $[\mathbf{5}-CO]^{\bullet+}$ is believed[2a] to correspond to a hydrogen-bridged structure $[CH_3O-H-O=CH_2]^{\bullet+}$. It can therefore be ruled out that the conventional isomers $\mathbf{2}^{\bullet+}$ and $\mathbf{3}^{\bullet+}$ as well as the latter two structures are formed upon ionization of dimethyl peroxide.

The structure of $[\mathbf{6}-CO]^{\bullet+}$ has not been studied further, but the CA mass spectrum resembles that of $[\mathbf{5}-CO]^{\bullet+}$ and is different from $\mathbf{1}^{\bullet+}$ as well. Upon ionization of **7** and **8** no significant intensities of $[C_2,H_6,O_2]^{\bullet+}$ were detected, indicating that decarbonylation of $\mathbf{7}^{\bullet+}$ and loss of ethene from $\mathbf{8}^{\bullet+}$, respectively, are of minor importance.

Second approach: Because neutralization and reionization achieved by high-energy collisions with target gas atoms or molecules are vertical processes,[37] the NR mass spectra[14] can provide a test for whether the ionic structure correlates with a stable neutral. Moreover, an intense recovery signal indicates that a neutral species with a geometry close to that of the ion exists. In the $^+NR^+$ experiment carried out with $\mathbf{1}^{\bullet+}$ radical cations the recovery signal represents the base peak (Figure 1).

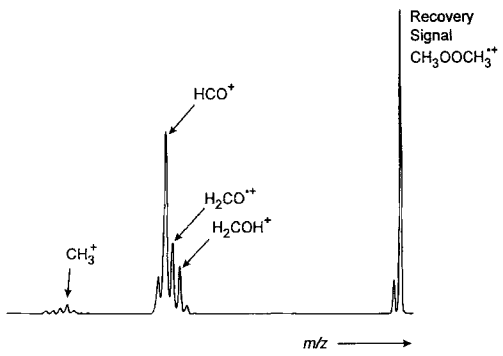

Figure 1. $^+NR^+$ mass spectrum (Xe, 80% T; O_2, 70% T) of the dimethyl peroxide radical cation $\mathbf{1}^{\bullet+}$.

From this finding, we conclude that hydrogen-bridged ions and ion/dipole complexes can most likely be ruled out, since for these structures the recovery signal is expected to be weak or even absent.[38] Similarly, distonic ions, such as CH_3-$OO^+(H)CH_2^{\bullet}$, are not expected to correspond to stable neutrals giving rise to an intense recovery signals.[39,40]

Third approach: The absolute intensity of the recovery signal of fully deuterated $\mathbf{1b}^{\bullet+}$ ions is higher than that for $\mathbf{1}^{\bullet+}$. A collisional activation experiment with the survivor ions[41] ($^+NR^+$/CA; Figure 2a) can thus be performed, in order to characterize the ion structure after the neutralization–reionization process. A comparison with the CA mass spectrum (Figure 2b) recorded in the same field-free region reveals that the structure-indicative region is similar in both spectra. Slight differences in the intensities of the DCO^+ ion relative to CD_2OD^+ are probably due to

0947-6539/97/0304-0628 $ 17.50+.50/0 Chem. Eur. J. 1997, 3, No. 4

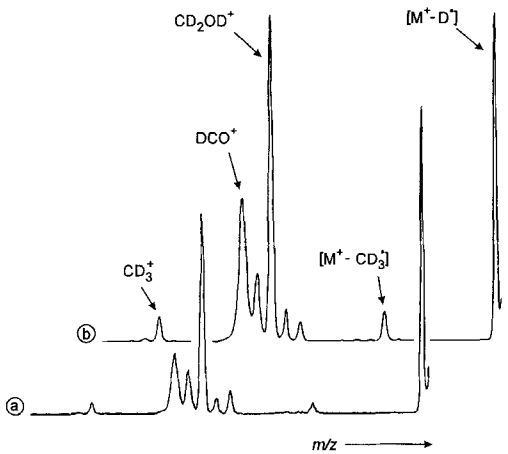

Figure 2. a) $^{+}NR^{+}$/CA mass spectrum (Xe, 80% T; O_2, 80% T; He, 80% T) of $\mathbf{1b}^{\bullet+}$. These ions were generated by neutralization–reionization of B(1)/E(1) mass-selected $\mathbf{1b}^{\bullet+}$, followed by mass-selection of the recovery ions with B(2); the spectrum was recorded by scanning E(2). b) CA mass spectrum (He, 80% T) of $\mathbf{1b}^{\bullet+}$. The ions were mass-selected using B(1)/E(1)/B(2), and the spectrum was recorded by scanning the second electrostatic sector E(2).

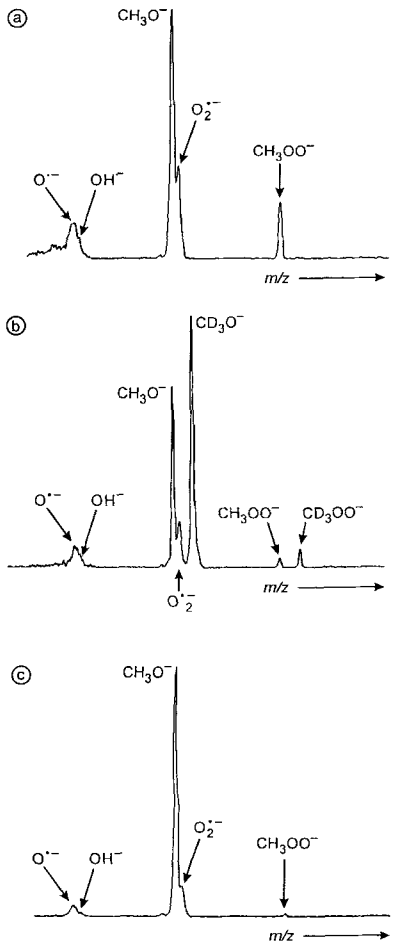

Figure 3. a) $^{-}CR^{-}$ mass spectrum (benzene, 70% T) of $\mathbf{1}^{\bullet+}$. b) $^{+}CR^{-}$ mass spectrum (benzene, 70% T) of $\mathbf{1a}^{\bullet+}$. c) $^{-}NR^{-}$ mass spectrum of $\mathbf{1}^{\bullet+}$ (Xe, 80% T; benzene, 70% T). Due to sensitivity, these spectra were performed with cations mass selected by B(1) only, and the resulting anions were monitored with E(1).

differences in the internal energy content, because CD_2OD^+ decomposes to $DCO^+ + D_2$, provided that sufficient internal energy is available.[42] Indeed, a comparison of the MI and the CA mass spectra of unlabeled $\mathbf{1}^{\bullet+}$ reveals that it is the HCO^+ ion ($\Delta m = 33$), that is most sensitive to changes in internal energy (Table 1): In the MI spectrum, HCO^+ is observed with an intensity of less than 1%, while it represents the third-most intense process in the CA spectrum (see below). Thus, the NR/CA experiment leads to the conclusion that the ion beam is essentially pure and the structure of the $[C_2,H_6,O_2]^{\bullet+}$ ion generated by electron ionization of **1** is the same prior to and after the neutralization/reionization process.

Fourth approach: At a certain stage of the present study, it became necessary to evaluate to what extent $\mathbf{1}^{\bullet+}$ can undergo degenerated hydrogen migration prior to other rearrangements. To this end, the cation structure was probed by charge reversal to anions ($^{+}CR^{-}$). In the $^{+}CR^{-}$ spectrum (Figure 3a), the anionic fragments CH_3O^-, $O_2^{\bullet-}$, and CH_3OO^- clearly indicate the integrity of the peroxide skeleton upon ionization. Moreover, the same experiment performed with $\mathbf{1a}^{\bullet+}$ (Figure 3b) leads to CH_3O^-, CD_3O^-, $O_2^{\bullet-}$, CH_3OO^-, and CD_3OO^-, but no other isotopologues; this clearly demonstrates that the methyl groups in $\mathbf{1}^{\bullet+}$ remain intact, and an H/D equilibration between the two methyl groups can thus be ruled out.

In the comparison of the $^{+}CR^{-}$ spectrum of $\mathbf{1}^{\bullet+}$ (Figure 3a) with the corresponding $^{+}NR^{-}$ spectrum (Figure 3c), distinct differences are observed: The CH_3O^- signal is much less intense relative to the other fragments in the $^{+}CR^{-}$ experiment than in the $^{+}NR^{-}$ spectrum (e.g., CH_3O^-:CH_3OO^- is ca. 4:1 in the $^{+}CR^{-}$ and ca. 70:1 in the $^{+}NR^{-}$ mass spectrum). While direct two-electron reductions without the formation of a short-lived neutral intermediate are feasible in the $^{+}CR^{-}$ experiment, in a $^{+}NR^{-}$ experiment two consecutive one-electron reductions must occur. Thus, charge reversal leads to fragmentations that reflect the properties of the cation, namely, its relatively strong O–O bond and its weakened C–O bond (see below). Therefore, fragments with an intact O–O bond are more intense in the $^{+}CR^{-}$ spectrum than in the $^{+}NR^{-}$ spectrum. In neutral CH_3OOCH_3 the peroxidic O–O bond is weak; consequently, CH_3O^- prevails the $^{+}NR^{-}$ mass spectrum, owing to O–O bond fission at the neutral stage followed by reionization of the fragments.

These experiments suggest that dimethyl peroxide remains structurally intact upon ionization and that the ion beam consists of $CH_3OOCH_3^{\bullet+}$. However, the decomposition reactions observed in the MI and CA mass spectra can also be explained in terms of the isomeric structure $\mathbf{4}^{\bullet+}$. Although the CH_3OO^-, HO_2^-, and $O_2^{\bullet-}$ fragments observed in the $^{+}CR^{-}$ experiment are convincing evidence for the existence of an O–O bond in the $[C_2,H_6,O_2]^{\bullet+}$ radical cation, we cannot exclude that minor amounts of $\mathbf{1}^{\bullet+}$ have undergone rearrangement to $\mathbf{4}^{\bullet+}$ (see below).

The optimized geometries of neutral and ionized dimethyl peroxide, derived at the BECKE3LYP/6-311++G** level of theory, are depicted in Figure 4. In line with previous ab initio calculations[43] and photoelectron spectroscopy,[44] for neutral **1** the conformation of minimum energy is C_{2h}-symmetric **1** corresponding to a *trans*-conformation; no *cis*- or *gauche*-conformers could be localized. Due to the extremely flat potential-energy surface for dihedral COOC angles in the range of ca. 120 to

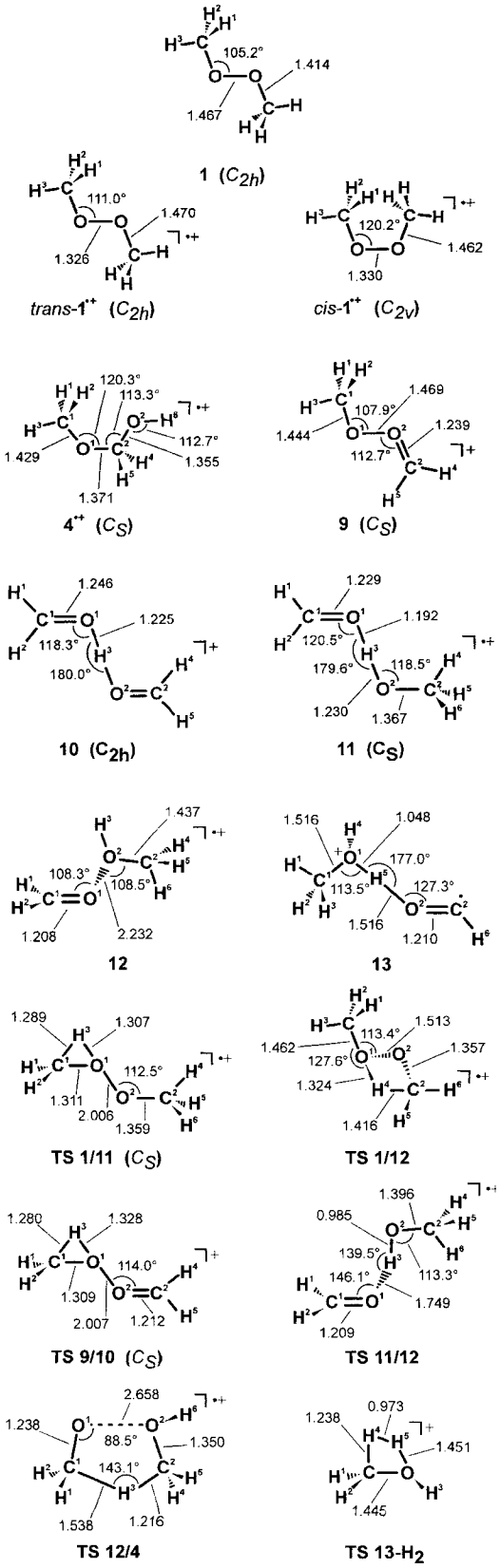

Figure 4. Optimized geometries of neutral and ionized dimethyl peroxide, derived at the BECKE3LYP/6-311++G** level of theory.

180°, several experimental[45] and theoretical[46] studies reported torsion angles smaller than 180°. However, it is not the aim of this work to resolve this uncertainty, and we will use the *trans*-structure **1** for a qualitative discussion, particularly since the other geometric parameters (i.e., bond lengths and angles) are in good agreement with those reported previously.[43–45] For the radical cation, two conformers have been located on the potential energy surface, C_{2h} symmetric *trans*-**1**$^{\bullet+}$ and *cis*-**1**$^{\bullet+}$ with C_{2v} symmetry, the latter being ca. 10 kcal mol^{-1} higher in energy. While we have not further pursued the search for a neutral counterpart of *cis*-**1**$^{\bullet+}$, the geometries of **1** and *trans*-**1**$^{\bullet+}$ are quite close to each other, and all of the slight changes in the bond lengths and angles can be traced back to the missing electron in *trans*-**1**$^{\bullet+}$. In particular, the O–O bond is shortened from 1.467 Å (neutral) to 1.326 Å in the radical cation, owing to the reduced repulsion between the nonbonding electron pairs at the oxygen atoms in the radical cation. The existence of a *trans*- and a *cis*-isomer of **1**$^{\bullet+}$ implies a partial double-bond character of the O–O bond due to delocalization of the unpaired electron with one of the free electron pairs of the adjacent oxygen atom. The relative energies for **1** and *trans*-**1**$^{\bullet+}$ (Table 2) lead to an adiabatic ionization energy IE_a(**1**) of 9.02 eV (207.8 kcal mol^{-1}), which is in excellent agreement with the experimental value (IE_a = 9.1 eV).[48]

Table 2. Calculated total energies (E_{total}), zero-point vibrational energies (ZPVE), and experimental heats of formation (ΔH_f) of $[C_2,H_6,O_2]^{\bullet+}$ isomers and relevant fragments.

	E_{total} [a] (hartree)	ZPVE (hartree)	ΔH_f [b] (kcal mol^{-1})	ΔH_f [c] (kcal mol^{-1})
1	−230.153115	0.081793	−26.2	−30.0
trans-**1**$^{\bullet+}$	−229.822067	0.081695	181.6	179.8
cis-**1**$^{\bullet+}$	−229.804609	0.080884	192.5	
4$^{\bullet+}$	−229.892955	0.080509	139.1	
9	−229.236097	0.070934	182.0	
9 + H$^{\bullet}$	−229.738354	0.070934	234.1	
10	−229.347394	0.066103	112.2	109.9 [47]
10 + H$^{\bullet}$	−229.849651	0.066103	164.3	162.0 [47]
11	−229.888983	0.074921	139.6	134.0 [d] [2a,e]
12	−229.888057	0.079487	140.2	149.9 [d] [2e]
13	−229.902655	0.079725	130.9	120.0 [d] [2a,e]
TS1/11	−229.759370	0.072337	220.9	
TS1/12	−229.742863	0.075036	231.3	
TS9/10	−229.217163	0.063618	193.9	
TS9/10 + H$^{\bullet}$	−229.719420	0.063618	246.0	
TS11/12	−229.883778	0.075850	142.8	
TS12/4	−229.851720	0.076304	163.0	
TS13-H_2	−115.898324	0.056492	199.3	
TS13-H_2 + HCO$^{\bullet}$	−229.776701	0.069446	210.0	
$CH_3OH_2^+$ + HCO$^{\bullet}$	−229.877338	0.076883	146.9	146.2
CH_3OH^+ + $CH_2OH^{\bullet}$	−229.847083	0.077538	165.9	161.8
CH_2OH^- + $CH_3O^{\bullet}$	−229.837784	0.076546	171.7	171.7
$CH_3OH^{\bullet+}$ + CH_2O	−229.839822	0.073494	170.4	175.3
$CH_3O^{\bullet+}$ + CH_3OH	−229.831578	0.074860	175.6	176.5
CH_3OH^+ + H_2 + HCO$^{\bullet}$	−229.829495	0.063493	176.9	178.7
CH_2OH^+ + H$^{\bullet}$ + CH_2O	−229.799216	0.066974	195.9	194.1
H$^{\bullet}$	−0.502257	0.0		52.1
H_2	−1.169509	0.010062		0.0
HCO$^{\bullet}$	−113.878377	0.012954		10.7
$CH_2O^{\bullet+}$	−114.117602	0.023838		224.7
CH_2O	−114.515350	0.026497		−26.0
CH_2OH^+	−114.781609	0.040477	168.6 [e]	168.0
$CH_2OH^{\bullet}$	−115.065474	0.037061	−9.5 [e]	−6.2
$^3CH_3O^+$	−114.667039	0.033136	240.5 [e]	247.4 [49a]
$CH_3O^{\bullet}$	−115.056175	0.036069	3.7 [e]	3.7
$CH_3OH^{\bullet+}$	−115.324472	0.046997		201.3
CH_3OH	−115.713976	0.051022		−48.2
$CH_3OH_2^+$	−115.998961	0.063929		135.5

[a] Total energies (0 K) based on BECKE3LYP/6-311++G**-optimized structures including ZPVE corrections. [b] Calculated on the basis of literature data for the CH_3OH^+ + $CH_3O^{\bullet}$ exit channel. [c] Unless stated otherwise, reference data have been taken from ref. [48]. [d] Calculated data. [e] Calculated relative to $CH_3O^{\bullet}$ as a reference.

0947-6539/97/0304-0630 $ 17.50+.50/0 Chem. Eur. J. 1997, 3, No. 4

Neutralization and reionization of a fast beam of particles in the NR experiments represent vertical processes,[37] and the process is favorable if the equilibrium geometries of neutral and cation do not differ much. Therefore, the structural similarity of **1** and *trans*-$\mathbf{1}^{\bullet+}$ easily explains the large intensity of the recovery signal in the $^{+}NR^{+}$ experiment. Furthermore, the vertical ionization energy of **1** ($IE_v = 9.7$ eV) measured by photoelectron spectroscopy[48] exceeds IE_a by 0.6 eV, further emphasizing the structural similarity of **1** and $\mathbf{1}^{\bullet+}$. Thus, both the ab initio theory and NR experiments strongly support our assignment that dimethyl peroxide remains intact upon ionization. Further, we can safely conclude that **1** generated in the course of the NR procedures corresponds to intact dimethyl peroxide, and these results provide us with a well defined starting point for the discussion of the unimolecular fragmentations as observed in the MI mass spectra.

Energetic considerations: Before discussing the metastable ion decompositions, some energetic arguments should be considered (Table 2):

1) A simple estimation[43b,48,49] shows that the bond dissociation energy (BDE) of the O–O bond of $\mathbf{1}^{\bullet+}$ ($BDE(CH_3O^{+}-{}^{\bullet}OCH_3) \approx 75$ kcal mol^{-1}) is drastically increased as compared to its neutral counterpart ($BDE(CH_3O-OCH_3) = 37$ kcal mol^{-1}).[50] This change is reflected in the O–O bond length, which is shorter in the radical cation (see above). In contrast, the C–O bond[51] weakens upon ionization ($BDE(CH_3-OOCH_3) = 87$ kcal mol^{-1}, $BDE(CH_3^{+}-{}^{\bullet}OOCH_3) = 77$ kcal mol^{-1}). Finally, the C–H bond strength $BDE(H\text{-}CH_2OOCH_3)$ can be estimated to ca. 95 kcal · mol^{-1}[52] for the neutral peroxide, while it is much lower for the cation ($BDE(H^{\bullet}-{}^{+}CH_2OOCH_3) = 52.5$ kcal mol^{-1}). With respect to the experimental $BDE(H^{\bullet}-{}^{+}CH_2OOH)$ of 33 kcal mol^{-1} for ionized methyl hydroperoxide,[50] the latter value may even be somewhat overestimated with BECKE3LYP, although the general agreement between experimental and calculated energetics is quite satisfactory. From these data we conclude that for neutral **1** the O–O bond defines an upper limit for the energy requirements of any conceivable decomposition channel (37 kcal mol^{-1}), while the unimolecular decay of $\mathbf{1}^{\bullet+}$ cannot involve fragmentation reactions with energy requirements above that for C–H bond fission (52 kcal mol^{-1}).

2) The heat of formation of ionized dimethyl peroxide has been computationally determined to be $\Delta H_f(\mathbf{1}^{\bullet+}) = 181.6$ kcal mol^{-1} (exp.: 179.8 kcal mol^{-1})[48] and by far exceeds that of most rearranged ions, such as $\mathbf{3}^{\bullet+}$ ($\Delta H_f = 141.7$ kcal mol^{-1}).[48] Moreover, the hydrogen-bridged radical cations $[CH_3O-H-OCH_2]^{\bullet+}$ (**11**) and $[CH_3O(H)-H-OCH]^{\bullet+}$ (**12**) are thermochemically even more favorable species. In other words, once rearranged $\mathbf{1}^{\bullet+}$ may give rise to several "hot" $[C_2,H_6,O_2]^{\bullet+}$ isomers, and it remains questionable, whether the ground-state energy profile represents an adequate description for the reactions of these rovibrationally highly excited intermediates (see below).

3) Although thermochemically high in energy, $\mathbf{1}^{\bullet+}$ must reside in a relatively deep well of the $[C_2,H_6,O_2]^{\bullet+}$ potential-energy surface, since otherwise rearrangements to isomeric structures are expected to occur. As this is not observed experimentally, substantial barriers must be associated with the first step of any conceivable isomerization. On one hand, these must be situated below the C–H bond dissociation limit, but on the other hand have to be high enough to kinetically stabilize the dimethyl peroxide radical cation. Moreover, these barriers further increase the amount of internal energy stored in any isomeric $[C_2,H_6,O_2]^{\bullet+}$ cation formed from $\mathbf{1}^{\bullet+}$.

On the basis of these results, it is not at all unreasonable to assume that the first step is rate-determining for every decomposition channel observed in the MI mass spectrum of $\mathbf{1}^{\bullet+}$, whereas the thermochemistry and barriers associated with subsequent reaction steps do not play an important role. These implications are in good agreement with the calculated potential-energy surface, which is presented in Figure 5. Indeed, $\mathbf{1}^{\bullet+}$ rests in a relatively deep well limited by a barrier for a 1,2-hydrogen migration via **TS1/11** (see below), which represents the reaction channel of lowest energy found by calculations and is located at an energy of 39.3 kcal mol^{-1} above the local minimum for $\mathbf{1}^{\bullet+}$.

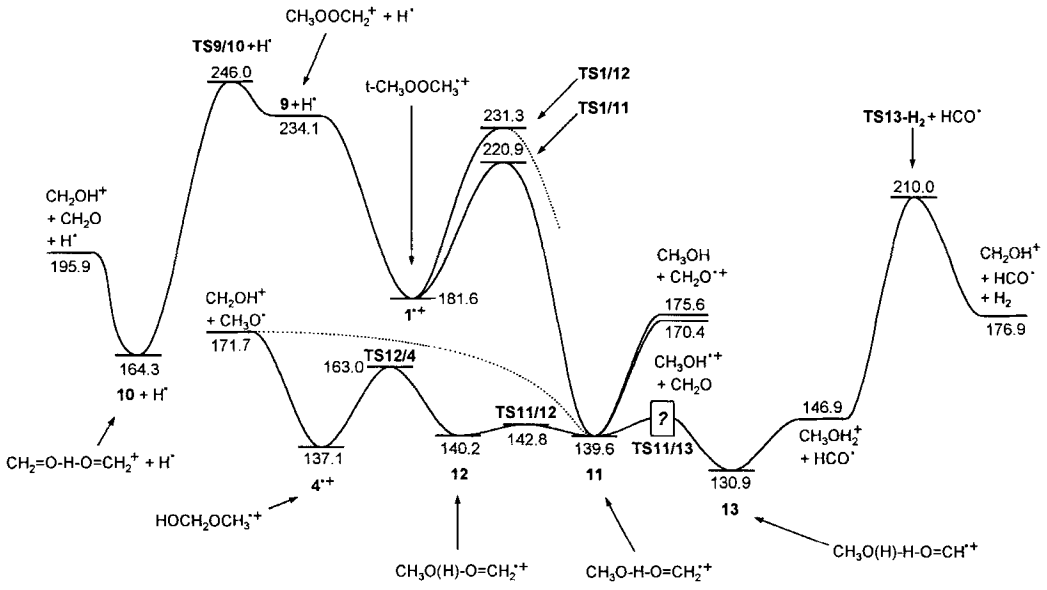

Figure 5. Calculated doublet potential-energy surface of the $[C_2,H_6,O_2]^{\bullet+}$ system at the BECKE3LYP/6-311++G** level of theory.

Metastable ion decomposition of dimethyl peroxide radical cations: Table 3 summarizes the data derived from the MI mass spectra of $\mathbf{1}^{\bullet+}$ and its isotopomers $\mathbf{1a}^{\bullet+}$ and $\mathbf{1b}^{\bullet+}$. Two major

Table 3. Mass differences (Δm in amu) observed in the MI mass spectra of dimethyl peroxide radical cations $\mathbf{1}^{\bullet+}$ – $\mathbf{1b}^{\bullet+}$ [a].

$-\Delta m =$	1	2	29	30	31	32	33	34	35	36	47	50
$\mathbf{1}^{\bullet+}$	60		2	2	28	7					1	
$\mathbf{1a}^{\bullet+}$	66	5	1	1	2	9	10	1	3		1	1
$\mathbf{1b}^{\bullet+}$		72		3		1		20		3		1

[a] Intensities are normalized to $\sum$reactions = 100%; intensities of less than 1% are omitted.

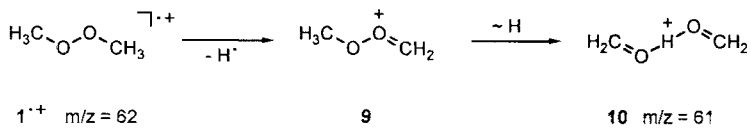

Scheme 1. Plausible reaction mechanism formation of the proton-bound dimer of formaldehyde from $\mathbf{1}^{\bullet+}$.

fragmentation reactions are observed for $\mathbf{1}^{\bullet+}$ within the μs time frame of metastable ion decompositions: 1) the loss of a hydrogen radical ($\Delta m = 1$), which corresponds to the base peak; and 2) formation of $[C,H_3,O]^+$ ions ($\Delta m = 31$). In addition, some minor processes contribute to the MI mass spectrum of $\mathbf{1}^{\bullet+}$, namely, the generation of protonated methanol ($\Delta m = 29$), methanol radical cations ($\Delta m = 30$), and ionized formaldehyde ($\Delta m = 32$). The elemental composition of these ions, if not straightforward, can be unequivocally derived by comparison of the MI mass spectra of $\mathbf{1}^{\bullet+}$ and $\mathbf{1b}^{\bullet+}$. The connectivities of the resulting product ions have been investigated by MI/CA experiments, which are presented here only as far as necessary for the investigation of mechanistic aspects of the decomposition processes of ionized dimethyl peroxide. Further, the similarity of the MI spectra of $\mathbf{1}^{\bullet+}$ and $\mathbf{1b}^{\bullet+}$, except for mass shifts arising from deuterium labeling, indicates that only small *inter*molecular kinetic isotope effects (KIE) are operative. Instead, from the ratio of H$^\bullet$ to D$^\bullet$ losses from $\mathbf{1a}^{\bullet+}$ an *intra*molecular KIE of $k_H/k_D \approx 13$ can be derived.[53] In the following, we will first concentrate on a discussion of the two major decomposition reactions, namely, loss of H$^\bullet$ and formation of $[C,H_3,O]^+$ ions.

The ionic product of the hydrogen atom loss from $\mathbf{1}^{\bullet+}$ has been structurally characterized by its MI/CA mass spectrum (Table 4), which exhibits loss of formaldehyde ($\Delta m = 30$) as the major reaction. In analogy, from both $[\mathbf{1a} - H]^+$ and $[\mathbf{1a} - D]^+$ the expulsions of $[D_0]$- and $[D_2]$formaldehyde ($\Delta m = 30, 32$) are observed with similar intensities. These findings point to the formation of the proton-bound dimer[54] of formaldehyde, which is confirmed by the CA mass spectrum of the independently generated proton-bound dimer of formaldehyde (Table 4).[55] Notably, the MI/CA mass spectrum of $[\mathbf{1} - H]^\bullet$ differs completely from that of protonated methyl formiate, which would arise as the ionic product from an α-cleavage of $\mathbf{4}^{\bullet+}$ (Table 4).

Scheme 1 presents a plausible reaction mechanism, which commences with a simple cleavage of an α-C–H bond giving rise to **9**. If one of the methyl hydrogen atoms migrates upon O–O bond cleavage, the proton-bound dimer **10** is formed, being lower in energy than its isomer **9** by 70 kcal mol^{-1}. Similar mechanisms have been found for higher dialkylperoxides, and for ionized di-*tert*-butyl peroxide an intermediate analogous to **9** has been suggested.[56] Recently, the gas-phase chemistry of the methyl hydroperoxide radical cation has been reported;[9c] in analogy to the process $\mathbf{1}^{\bullet+} \rightarrow \mathbf{9} + H^\bullet$, the molecular ion $CH_3OOH^{\bullet+}$ unimolecularly decomposes through α-cleavage to yield the protonated carbonyl oxide CH_2OOH^+ together with H$^\bullet$. However, the calculated energy demand of this process is rather high: abstraction of a hydrogen atom consumes about 50 kcal mol^{-1} (see above) and the transition-state structure **TS9/10** associated with 1,2-H shift requires additional 12 kcal mol^{-1}. Although all attempts failed to localize a transition-state structure for a direct process $\mathbf{1}^{\bullet+} \rightarrow \mathbf{10} + H^\bullet$, we cannot exclude that such a pathway exists and may circumvent the energetic problems imposed by the reaction $\mathbf{1}^{\bullet+} \rightarrow \mathbf{9} + H^\bullet \rightarrow \mathbf{10} + H^\bullet$.

In competition, the transition-state structure for the 1,2-H shift via **TS1/11** is located only ca. 40 kcal mol^{-1} above the minimum of the dimethyl peroxide radical cation. Although loss of a hydrogen atom is also feasible from other intermediates of the potential-energy surface depicted in Figure 5 (e.g. **11**), we believe that the α-cleavage process gives rise to the major fraction of $[\mathbf{1} - H]^+$ ions. Three arguments support this assumption:

1) The hydrogen losses from $\mathbf{1a}^{\bullet+}$ exhibit a large intramolecular KIE of ca. 13, which is not observed for the other reaction channels (Table 3). If, instead, the hydrogen loss would occur from one of the intermediates formed after the 1,2-H shift, **TS1/11** is expected to be rate-determining and the same KIE should affect all reaction channels observed. Since this is not found in the experiments, the hydrogen loss must correspond to a mechanistic pathway competing with the other decomposition processes.

2) The α-cleavage is a direct process and not hindered by a substantial barrier, so that, despite the higher energy demand, it can compete with the rearrangement via **TS1/11**. In addition, a

Table 4. Mass differences (Δm in amu) observed in the MI/CA mass spectra of the daughter ions formed by hydrogen atom loss from $\mathbf{1}^{\bullet+}$ – $\mathbf{1b}^{\bullet+}$ and the CA mass spectra of independently generated reference ions [a].

$-\Delta m =$	1	14	15	16	18	28	29	30	31	32	33	34	35	36	38	46	47	48	50
$[\mathbf{1}-H]^+$		2	7			3	4	100	5	34	5					2	1		
$[\mathbf{1a}-H]^+$		5			16	3	5	100	10	96	5	41	35	3		6	1		
$[\mathbf{1a}-D]^+$			12	4		6	4	100	6	85	25	23	3					3	1
$[\mathbf{1b}-D]^+$				4	12	6		3		100		10		38	2			4	1
$(CH_3O)_2H^+$ (CA) [b]		1	2			1	4	100	6	16	2					1	1		
$HC(OH)OCH_3^-$ (CA) [c]	13		3	13		100	4	15	5	28	2					8	1		

[a] Intensities are given relative to the base peak = 100%; processes of less than 1% are omitted. [b] The proton-bound dimer of formaldehyde was generated by chemical ionization of formaldehyde using methane as reagent gas. [c] Protonated methyl formiate was produced from chemical ionization of methyl formiate with methane as reagent gas.

0947-6539/97/0304-0632 $ 17.50+.50/0 Chem. Eur. J. 1997, 3, No. 4

Table 5. Mass differences (Δm in amu) observed in the MI/CA mass spectra of $[C,H_3,O]^+$ ions and their isotopologues generated by unimolecular fragmentation of metastable $\mathbf{1}^{\bullet+} - \mathbf{1b}^{\bullet+}$ [a].

	Mass of daughter ion	Assigned ion structure	*m/z* of fragment ion [b] 32	31	30	29	28	20	19	18	17	16	15	14	13	12
$[\mathbf{1}^{\bullet+} - 31]$	31	CH_2OH^+			15	100	12			0.3	0.5	0.1	<0.04	0.8	0.5	0.2
$[\mathbf{1a}^{\bullet+} - 34]$ [c]	31	CH_2OH^+			22	100	11			0.4	0.6	0.1	<0.01	0.8	0.4	0.2
$[\mathbf{1a}^{\bullet+} - 33]$	32	CH_2OD^+		15	100	45	16		0.2	0.4	<0.05	0.1	<0.08	0.6	0.3	0.1
$[\mathbf{1a}^{\bullet+} - 32]$	33	CD_2OH^+	10	17	100	20	11		0.1	<0.08	0.4	1.0	<0.09	0.4	<0.08	0.1
$[\mathbf{1a}^{\bullet+} - 31]$ [c]	34	CD_2OD^+	28		100		9	0.3	<0.01	0.6	<0.01	0.1	<0.02	0.5	<0.01	0.2
$[\mathbf{1b}^{\bullet+} - 34]$	34	CD_2OD^+	25		100		10	0.2	<0.03	0.4	<0.07	0.8	<0.04	0.4	<0.02	0.2

[a] Intensities are given relative to the base peak = 100%. [b] For the sake of clarity, *m/z* values are given here instead of Δm. [c] Owing to the low intensities of these ions, it was impossible to record MI/CA spectra with distinct signals in the structure-indicative region (*m/z* = 12–20). The data given here were derived from CA spectra of the corresponding ions extracted from the ion source. The hydrogen-loss regions (*m/z* = 28–32) are identical in the CA and the corresponding MI/CA spectra of $[\mathbf{1a}^{\bullet+} - 31]$.

comparison of the C–H bond dissociation energies of dimethyl peroxide and methyl hydroperoxide radical cations finally indicates that the energy demand for the hydrogen loss from $\mathbf{1}^{\bullet+}$ may be somewhat overestimated (see above).

3) The H$^\bullet$ loss channel represents an upper limit for the internal energy content of metastable $\mathbf{1}^{\bullet+}$, and the reaction $\mathbf{1}^{\bullet+} \rightarrow \mathbf{9}^+ + H^\bullet$ will certainly take place upon collisional activation. Thus, if unimolecular loss of H$^\bullet$ would not occur directly from metastable $\mathbf{1}^{\bullet+}$, but from a rearranged ion, the MI/CA should differ from the CA/CA mass spectrum of $[\mathbf{1} - H]^+$. This, is, however, not observed in the experiment, indicating that unimolecular as well as collision-induced loss of H$^\bullet$ occur from genuine $\mathbf{1}^{\bullet+}$.

As far as the second most intense fragmentation reaction of $\mathbf{1}^{\bullet+}$ is concerned, namely, the formation of $[C,H_3,O]^+$ ions, two isomers may be generated: CH_3O^+ in its triplet state or the thermochemically by far more stable CH_2OH^+.[50, 57] Theoretical results predict that $^1CH_3O^+$ collapses without any energy barrier to the protonated formaldehyde structure.[58] Our attempts to localize a $^1CH_3O^+$ species using the BECKE3LYP DFT/HF hybrid method confirms this result again, in that the geometry always converges to CH_2OH^+. In contrast, $^3CH_3O^+$ corresponds to a shallow minimum on the potential-energy surface with a low barrier for rearrangement to a CH_2OH^+ structure.[50] The heat of formation of the $^3CH_3O^+$ cation has been calculated (Table 2) to be 240.5 kcal mol^{-1} in agreement with earlier results,[49, 50] which reported $\Delta H_f(^3CH_3O^+) = 247 \pm 5$ and 245 ± 6 kcal mol^{-1}, respectively. Experimental evidence for the generation of $^3CH_3O^+$ ions has been provided by charge reversal experiments performed with CH_3O^- anions.[49] Direct cleavage of the O–O bond in $\mathbf{1}^{\bullet+}$ might lead to $^3CH_3O^+$ ions as well, and therefore, we studied the structure of unimolecularly generated *m/z* = 31 ions by MI/CA experiments (Table 5). However, the peaks at *m/z* = 14 and 17 within the structure-indicative region reveal that the $[C,H_3,O]^+$ ions have a CH_2OH^+ connectivity instead of CH_3O^+. For the latter, signals at *m/z* = 15 and 16 would have been expected, which are practically absent in the experiment.

Fraser and co-workers[6] measured the metastable transitions of $\mathbf{1}^{\bullet+}$ and postulated that the CH_2OH^+ ions are formed through an O–O bond fission, which gives rise to $CH_3O^\bullet$ radical losses, combined with a 1,2-hydrogen shift from carbon to oxygen. This reaction can either proceed through $^1[CH_3O]^+$, which may rearrange to protonated formaldehyde during the O–O bond cleavage (Scheme 2a), or through $^3[CH_3O]^+$, which may isomerize to CH_2OH^+ as well (Scheme 2b). However, initial cleavage of the O–O bond is not likely because its energy demand exceeds the limit defined by C–H bond homolysis of metastable $\mathbf{1}^{\bullet+}$. Thus, C–H bond fission should be achieved more easily than that of the O–O bond. In addition, according to Scheme 2 all hydrogen atoms of the CH_2OH^+ ions should stem from a single methyl group, so that $\mathbf{1a}^{\bullet+}$ should lead to CH_2OH^+ and CD_2OD^+, whereas predominantly CH_2OD^+ and CD_2OH^+ are observed experimentally. Similarly, rearrangement mechanisms leading from $\mathbf{1a}^{\bullet+}$ to isotopomers of $\mathbf{4}^{\bullet+}$ with intact methyl group can be ruled out (Scheme 2c), because, upon loss of a methoxyl radical, CH_2OH^+ ions would be generated, in which all hydrogen atoms also originate from a single methyl group.

The simultaneous formation of $[C,H_3,O]^+$, $[C,H_2,D,O]^+$, $[C,H,D_2,O]^+$, and $[C,D_3,O]^+$ ions (Δm = 31–34) from $\mathbf{1a}^{\bullet+}$ in

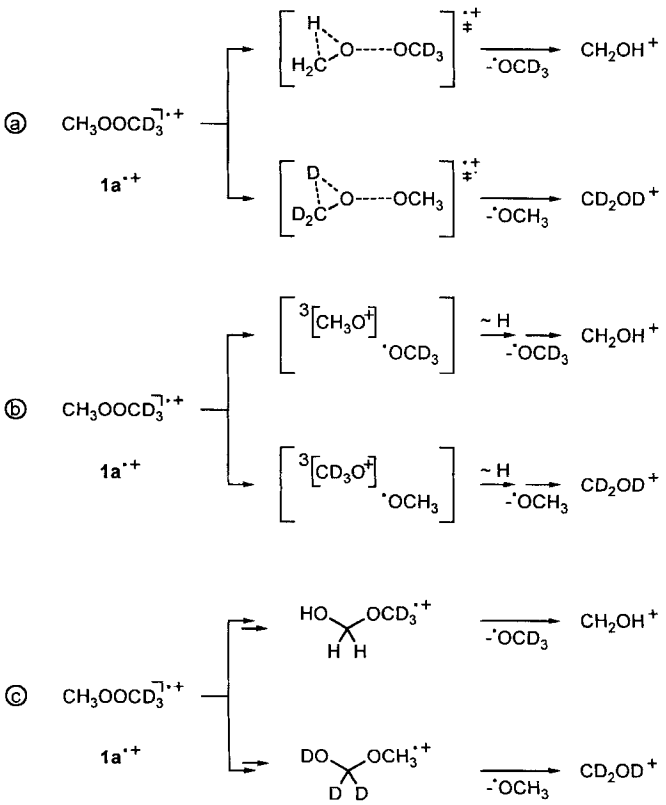

Scheme 2. Possible mechanisms for the decomposition of $\mathbf{1a}^{\bullet+}$.

a ca. 2:9:10:1 ratio (Table 3) seems to indicate an H/D-equilibration of all six hydrogen atoms in $\mathbf{1a}^{\bullet+}$ (statistical ratio: 1:9:9:1). However, inspection of the structure-indicative regions ($m/z = 12-20$) in the MI/CA mass spectra of these ions (Table 5) clearly disproves H/D equilibration, that is, $[\mathbf{1a}^{\bullet+} - 33]$ corresponds to CH_2OD^+ rather than $CHDOH^+$ (distinct signals for $m/z = 14$ and 16, while $m/z = 15$ and 17 are weak) and similarly $[\mathbf{1a}^{\bullet+} - 32]$ corresponds to CD_2OH^+ rather than $CHDOD^+$ (distinct signals for $m/z = 16$ and 17, while $m/z = 15$ and 18 are weak). Thus, the formation of $[C,H_3,O]^+$ must follow a more complex mechanistic scenario for the fragmentation of $\mathbf{1}^{\bullet+}$, which does not involve H/D exchange and provides an explanation for the isotope distribution observed.

Three possible stepwise fragmentations might lead from $\mathbf{1}^{\bullet+}$ to CH_2OH^+: 1) consecutive losses of H$^\bullet$ and CH_2O as suggested by the MI/CA mass spectrum of $[\mathbf{1} - H]^+$ (Scheme 3a), 2) formation of methanol cations by formaldehyde loss followed by an α-cleavage with concomitant expulsion of H$^\bullet$ (Scheme 3b), and 3) expulsion of HCO$^\bullet$ radicals giving rise to protonated methanol ions, which subsequently lose H_2 (Scheme 3c). Taking into account that the $\mathbf{1}^{\bullet+}$ ions must be rovibrationally excited prior to dissociation (see above), all

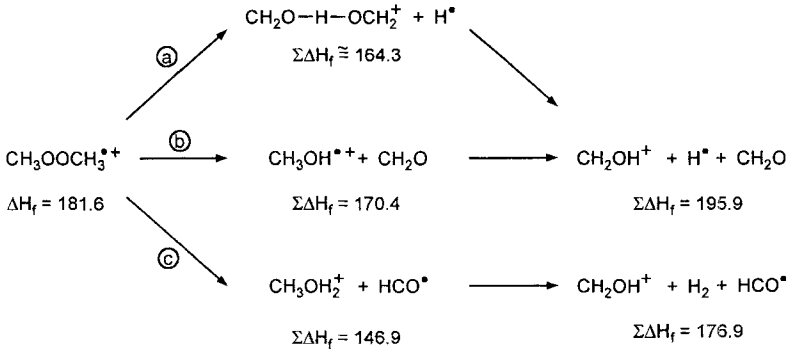

Scheme 3. Possible stepwise fragmentations leading from $\mathbf{1}^{\bullet+}$ to CH_2OH^+ (ΔH_f values in kcal mol^{-1}).

three mechanisms are accessible as far as thermochemistry is concerned. However, neither MI/MI experiments nor the ion-retardation method provide any indications that might point to a consecutive mechanism. Moreover, pathway a can be safely excluded from the kinetic energy release (KER) values, $T_{0.5}$ (Table 6). The hydrogen atom loss channel is associated with a substantially higher KER ($T_{0.5} = 27.5 \pm 2$ m eV) than the formation of CH_2OH^+ ions ($T_{0.5} = 9.5 \pm 2$ m eV). In addition, in path a one would expect that the kinetic isotope effect observed for the H$^\bullet$ and D$^\bullet$ losses should be reflected in the subsequent formaldehyde losses as well. In contrast to the experimental findings, this would lead to substantially higher abundances of CH_2OD^+ ($m/z = 32$) and CD_2OD ($m/z = 34$) ions formed from $[\mathbf{1a} - H]^+$ as compared to CH_2OH^+ ($m/z = 31$) and CD_2OH^+ ($m/z = 33$), which are generated from $[\mathbf{1a} - D]^+$. The reaction sequence c (Scheme 3c) is not likely on thermochemical grounds, since the elimination of H_2 from $CH_3OH_2^+$ after HCO$^\bullet$ loss via **TS13-H$_2$** is hindered by a huge barrier (Figure 5).

In order to further substantiate these arguments, CIDI mass spectra were performed aimed at the characterization of the neutrals expelled unimolecularly from $\mathbf{1}^{\bullet+}$. If the CH_2OH^+ ions are formed in a direct rather than a consecutive process, two different neutrals with a mass of 31 amu may be formed: methoxyl radicals, $CH_3O^\bullet$, or the thermochemically more favorable hydroxymethyl radicals, $^\bullet CH_2OH$. In the CIDI experiment, neutrals cogenerated in dissociations are ionized by high-energy collisions with oxygen as target gas. The ionization process performed with $^\bullet CH_2OH$ radicals is known[13] to give rise to an intense CH_2OH^+ signal ($m/z = 31$) and fragments at $m/z = 14$ ($CH_2^{\bullet+}$) and 17 (OH^+), while peaks for CH_3^+ and $O^{\bullet+}$ ($m/z = 15$, 16) are hardly seen. Instead, upon ionization, $CH_3O^\bullet$ radicals lead to CH_3O^+ ions, which spontaneously give rise to HCO^+ and fragment signals for CH_3^+ and $O^{\bullet+}$, respectively.[13, 49] In the CIDI mass spectrum (Figure 6) the HCO^+ signal represents

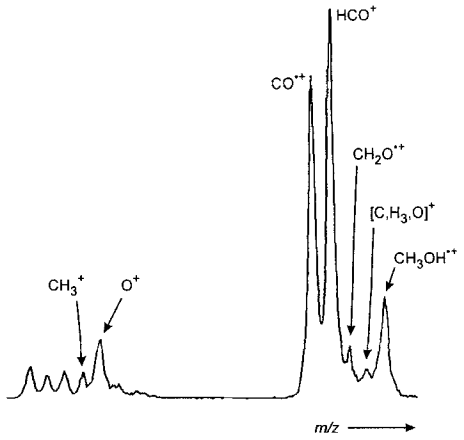

Figure 6. Partial CIDI mass spectrum (O_2, 60% T, $m/z = 11-33$) of the neutrals generated unimolecularly from $\mathbf{1}^{\bullet+}$ in the field-free region between E(1) and B(2); contribution of $^+NR^+$ processes to the CIDI spectrum are negligible.

the base peak and only a very small peak at $m/z = 31$ is observed. Remarkably, the $O^{\bullet+}$ signal ($m/z = 16$) is the most intense peak in the structure-indicative region, and a signal for CH_3^+ is also clearly present; note, however, that interferences with the minor amounts of neutral CH_2O and CH_3OH formed unimolecularly cannot be excluded, but, owing to their low intensities, these were not considered as important. Thus, we conclude from the CIDI mass spectrum that $CH_3O^\bullet$ radicals are formed upon unimolecular decay of $\mathbf{1}^{\bullet+}$. If, instead, $^\bullet CH_2OH$ radicals, which are thermochemically more stable by ca. 10 kcal mol^{-1},[48] were formed, one should expect a much more distinct signal at $m/z = 31$ in the CIDI mass spectrum of $\mathbf{1}^{\bullet+}$, because ionization of hydroxymethyl radical is facile.[13]

Another approach to the reactivity of $[C_2,H_6,O_2]^{\bullet+}$ radical cations is the reaction of ionized formaldehyde with methanol, which first form an encounter complex located on the $[C_2,H_6,O_2]^{\bullet+}$ potential-energy surface. In order to differentiate

Table 6. Kinetic energy release (KER) values. $T_{0.5}$, for the metastable ion decomposition processes of $\mathbf{1}^{\bullet+}$ estimated from peak half-height widths.

Process	Δm	$T_{0.5}$ [meV]
$\mathbf{1}^{\bullet+} \rightarrow (H_2CO)_2H^+ + H^\bullet$	1	27.5 ± 2
$\mathbf{1}^{\bullet+} \rightarrow CH_3OH_2^+ + HCO^\bullet$	29	7.7 ± 4
$\mathbf{1}^{\bullet+} \rightarrow CH_3OH^{\bullet+} + H_2CO$	30	9.8 ± 6
$\mathbf{1}^{\bullet+} \rightarrow CH_2OH^+ + CH_3O^\bullet$	31	9.5 ± 2
$\mathbf{1}^{\bullet+} \rightarrow CH_2O^{\bullet+} + CH_3OH$	32	10.3 ± 2

0947-6539/97/0304-0634 $ 17.50+.50/0 Chem. Eur. J. 1997, 3, No. 4

between the two reacting partners, we studied the reaction of $CH_2O^{\bullet+}$ with CD_3OH under Fourier-transform ion cyclotron resonance (FT-ICR) conditions. In agreement with previous results,[59] this reaction yields CD_2OH^+, $CD_3OH^{\bullet+}$, and $CD_3OH_2^+$ ions, which are all observed in the MI mass spectra of $\mathbf{1a}^{\bullet+}$ as well. Owing to the different internal energy contents of the encounter complex compared to rearranged $\mathbf{1}^{\bullet+}$ ions, the intensity distribution differs in the two experiments. Further, no CH_2OD^+ is formed, which is again in line with the loss of a $CH_2DO^{\bullet}$ radical instead of isomeric $^{\bullet}CH_2OD$. In contrast, a [$^{\bullet}CH_2OD/CD_2OH^+$] ion/dipole complex should lead to CD_2OH^+ *and* CH_2OD^+, because a degenerate electron transfer would be facile. Thus, we conclude that the ion–molecule reaction of $CH_2O^{\bullet+}$ with CD_3OH and the unimolecular decay of $\mathbf{1}^{\bullet+}$ proceed via common reaction intermediates.

At this point, we return to the ab initio result (Figure 4 and 5). Metastable $\mathbf{1}^{\bullet+}$ can undergo two different hydrogen shifts: 1) 1,2-H migration (**TS1/11**) associated with a barrier of ca. 30 kcal mol^{-1} which is typical[2e, 8, 39e–f, 60] for many proton transfers in radical cations, and 2) a 1,3-H transfer[61] (**TS1/12**) which is more energy demanding by 10 kcal mol^{-1}. Although the 1,3-H migration leads to an attractive intermediate **12** for the rationalization of the observed label distributions, this pathway is unlikely on energetic grounds, because it is very close to the energetic limit given by C–H bond homolysis in $\mathbf{1}^{\bullet+}$. Thus, the unimolecular fragmentation of $\mathbf{1}^{\bullet+}$ is most probably governed by a competition between direct C–H bond fission and a 1,2-H transfer.

All attempts to localize a stationary point for the $^{\bullet}CH_2$-$O^+(H)$–OCH_3 distonic ion as the product of 1,2-H transfer on the potential-energy surface failed, and in order to determine the minima that are connected by **TS1/11**, we followed the intrinsic reaction coordinate with the IRC method introduced by Gonzalez and Schlegel;[36] we found that **TS1/11** leads from $\mathbf{1}^{\bullet+}$ to the hydrogen-bridged radical cation **11** as a central intermediate. Note that **11** is no less than 42 kcal mol^{-1} more stable than $\mathbf{1}^{\bullet+}$ and even 81.3 kcal mol^{-1} below **TS1/11**; this means that **11** is rovibrationally excited by more than 80 kcal mol^{-1}, if it is generated from metastable $\mathbf{1}^{\bullet+}$. The radical cation **11** is connected with the $[CH_3OH/CH_2O]^{\bullet+}$ ion/dipole complex **12** by a very small barrier of only 3.2 kcal $\cdot$mol^{-1} (**TS11/12**), so that these ions will interconvert easily. Note that **12** had earlier been assigned as a transition-state structure;[2e] however, with BECKE3LYP **11** and **12** are well-defined minima, which represent plausible structures for the encounter complexes formed from ionized formaldehyde and methanol in the FT-ICR and rationalize the observation of common product ions in both experimental approaches (see above). However, the MI mass spectrum of **11**, when generated independently from methyl glycolate, exhibits losses of HCO$^{\bullet}$ radicals concomitant with $CH_3OH_2^+$ (m/z = 33) as major reaction channel, while formation of CH_2OH^+ (m/z = 31) is much less prominent. These enormous differences in the intensities of these two channels can be traced back to the internal energy effects, because, when formed from methyl glycolate, the internal energy of **11** is much lower than when generated from $\mathbf{1}^{\bullet+}$.

In order to explain the observed protonated formaldehyde ions and the isotope distribution found for $\mathbf{1a}^{\bullet+}$, a second hydrogen shift from the intact methyl group to the other half of the molecule must proceed prior to dissociation of **11** or **12**. Indeed, we could localize a transition-state structure in which one of the methyl hydrogen atoms is transferred to the other carbon and which is 22.8 kcal mol^{-1} higher in energy than **12** (Table 2). Formally, this migration would lead to the $^{\bullet}CH_2O^+(H)$–OCH_3 distonic ion; however, as stated above, this ion could not be located by ab initio theory. Further, the extremely long O–O bond discounts this proposal. Therefore, we propose that hydrogen transfer is followed by migration of the newly formed CH_3O moiety to the second carbon atom yielding $\mathbf{4}^{\bullet+}$; we therefore denote the transition-state structure as **TS12/4**. There may exist other low-energy pathways for hydrogen migrations in **11** and **12**, for example, a multicentered TS leading directly from **11** to $\mathbf{4}^{\bullet+}$. However, we have not studied this aspect in further detail, because the generation of $\mathbf{4}^{\bullet+}$ via **TS12/4** is not too energetic and accounts for the experimental findings: The methyl group of so-formed $\mathbf{4}^{\bullet+}$ bears two hydrogen atoms from the first and one hydrogen atom from the second methyl group in $\mathbf{1}^{\bullet+}$, and the same applies for the hydroxymethyl functionality. As a consequence, expulsion of methoxyl radicals from $\mathbf{4}^{\bullet+}$, formed in the sequence $\mathbf{1}^{\bullet+} \rightarrow \mathbf{11} \rightarrow \mathbf{12} \rightarrow \mathbf{4}^{\bullet+}$, explains the isotope distribution found for $\mathbf{1a}^{\bullet+}$. This mechanistic scenario is presented in Scheme 4 for labeled $\mathbf{1a}^{\bullet+}$, and the isotope distribution observed in the MI mass spectra is reproduced correctly, if one assumes that the minor contribution of CH_2OH^+ and

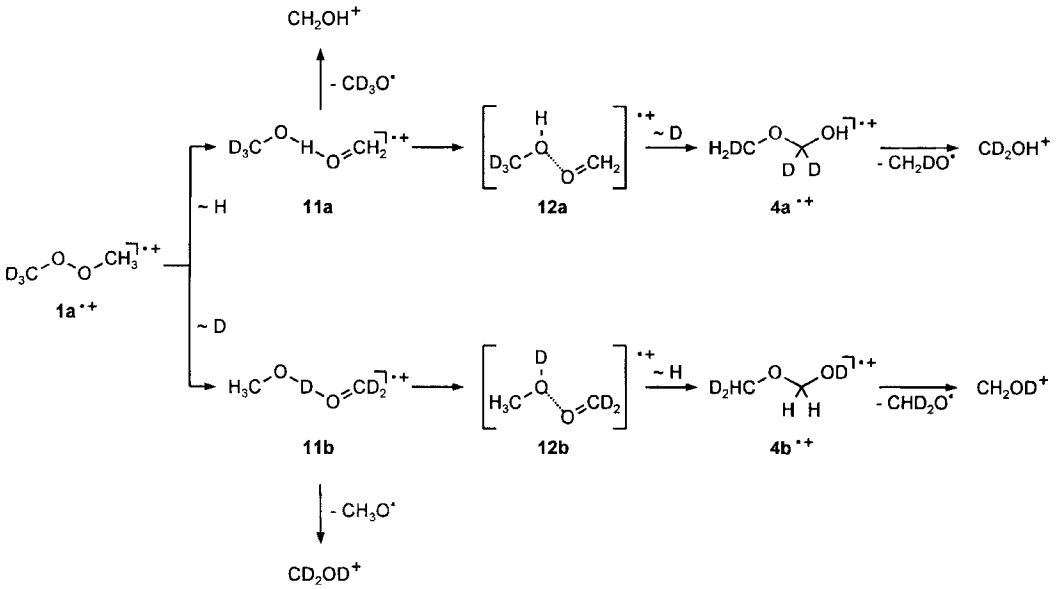

Scheme 4. Mechanism of fragmentation of $\mathbf{1a}^{\bullet+}$.

CD_2OD^+ ions are due to direct cleavage of the hydrogen bond in **11**. Finally, the nonoccurrence of statistical H/D exchange can be attributed to the enormous amount of internal energy in **11**, **12**, or $\mathbf{4}^{\bullet+}$ when formed from metastable $\mathbf{1}^{\bullet+}$, so that the respective lifetimes are shortened drastically.

As far as the minor processes in the MI mass spectrum of $\mathbf{1}^{\bullet+}$, namely, generation of $CH_2O^{\bullet+}$, $CH_3OH^{\bullet+}$, and $CH_3OH_2^+$, are concerned, these can be easily explained from the intermediates presented so far. Formaldehyde and methanol radical cations can be formed upon fission of, for example, the weak O–O bond in **12** or the hydrogen bridge in **11**. The loss of HCO$^\bullet$ radicals ($\Delta m = 29$) concomitant with formation of protonated methanol most likely involves another hydrogen-bridged radical cation, **13**, which is believed to represent the global minimum of the $[C_2,H_6,O_2]^{\bullet+}$ potential-energy surface. By means of ab initio methods, we could not localize a transition-state structure for the reaction **11** → **13** (Figure 5); however, it is obvious that **13** can be reached from rovibrationally excited **11**. Finally, by combining the experimental and theoretical results, we can provide an overview of the unimolecular decomposition pathways of $\mathbf{1}^{\bullet+}$ (Scheme 5).

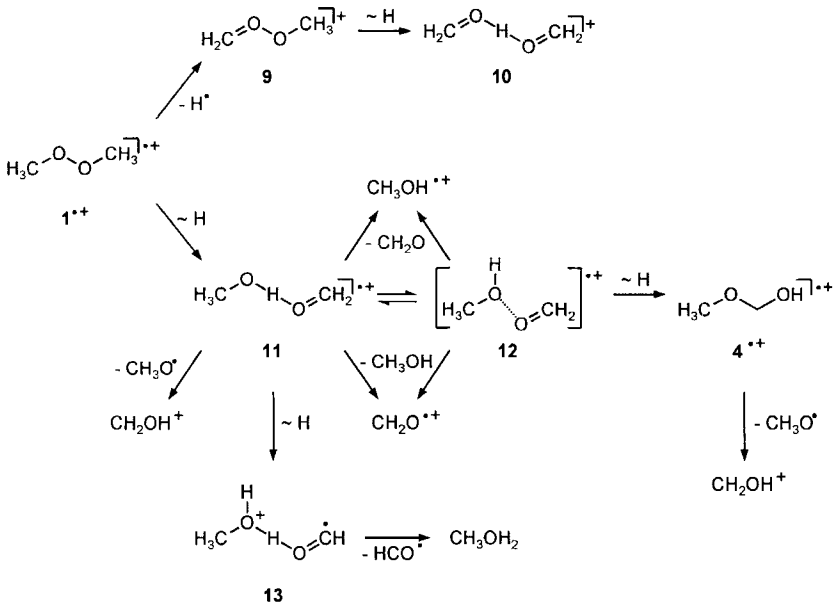

Scheme 5. Overview of the unimolecular decomposition pathways of $\mathbf{1}^{\bullet+}$.

Conclusions

The present study of dimethyl peroxide radical cation demonstrates how mass spectrometry and ab initio methods provide complementary tools for the elucidation of ion structures as well as reaction mechanisms in the gas phase. In this respect, the accuracy of the economic BECKE3LYP approach is particularly promising. Compared to the previous studies of the $[C_2,H_6,O_2]^{\bullet+}$ potential-energy surface,[2] the dimethyl peroxide radical cation reveals some intriguing features:

1) Except for a significant O–O bond shortening, the structure of the molecular ion is nearly the same as the neutral.
2) The cation, though high in energy, is kinetically stabilized, and the structure is preserved until decomposition.
3) All rearrangement products are much lower in energy and are generated as highly excited species with a chemistry distinctly different from low-energy analogues.
4) All observed exit channels are lower in energy than the peroxide radical cation. However, despite this high-energy situation, one of the major reaction channels involves a surprisingly specific double hydrogen transfer, which is hardly subject to H/D exchange processes.

Finally, the good agreement between experiment and theory which is obtained in this study, points to a much more general question: To what extent does the calculated ground-state potential-energy surfaces really describe the unimolecular dissociation of $\mathbf{1}^{\bullet+}$, given that ions with rather high internal energies are invoked as intermediates? For example, why does intermediate **11** not simply spontaneously dissociate, instead of undergoing a specific hydrogen transfer prior to fragmentation? Obviously, these phenomena are due to dynamic effects, which are not covered at all by a ground-state picture. Moreover, the experimentally observed degree of selectivity suggest that dynamic effects may play crucial roles, not only in mass spectrometric fragmentations, but also in other high-energy processes, such as combustion phenomena.

Appendix

For the sake of clarity, in Figure 4 we reduced the calculated geometrical data for the $[C_2,H_6,O_2]^{\bullet+}$ ions to the important features of the ion structures. Here, the complete set of data is given (bond lengths in Å, bond angles in degrees). Numbers of atoms are used as shown in Figure 4.

1: C_{2h} symmetry; $r(OO) = 1.467$; $r(CO) = 1.414$; $r(CH^1) = 1.095$; $r(CH^3) = 1.092$; $\sphericalangle COO = 105.2$; $\sphericalangle H^1CO = 111.2$; $\sphericalangle H^3CO = 104.6$; $\sphericalangle H^1CH^2 = 109.6$; $\sphericalangle H^1CH^3 = 109.6$; $\sphericalangle COOC = 180.0$; $\sphericalangle H^1COO = 61.5$; $\sphericalangle H^3COO = 180.0$

trans-$\mathbf{1}^{\bullet+}$: C_{2h} symmetry; $r(OO) = 1.326$; $r(CO) = 1.470$; $r(CH^1) = 1.091$; $r(CH^3) = 1.088$; $\sphericalangle COO = 111.0$; $\sphericalangle H^1CO = 107.9$; $\sphericalangle H^3CO = 102.8$; $\sphericalangle H^1CH^2 = 112.2$; $\sphericalangle H^1CH^3 = 112.7$; $\sphericalangle COOC = 180.0$; $\sphericalangle H^1COO = 60.7$; $\sphericalangle H^3COO = 180.0$

cis-$\mathbf{1}^{\bullet+}$: C_{2v} symmetry; $r(OO) = 1.330$; $r(CO) = 1.462$; $r(CH^1) = 1.092$; $r(CH^3) = 1.089$; $\sphericalangle COO = 120.2$; $\sphericalangle H^1CO = 109.4$; $\sphericalangle H^3CO = 101.6$; $\sphericalangle H^1CH^2 = 112.2$; $\sphericalangle H^1CH^3 = 112.7$; $\sphericalangle COOC = 0.0$; $\sphericalangle H^1COO = 61.8$; $\sphericalangle H^3COO = 180.0$

$\mathbf{4}^{\bullet+}$: C_s symmetry; $r(C^1O^1) = 1.429$; $r(O^1C^2) = 1.371$; $r(C^2O^2) = 1.355$; $r(C^1H^1) = 1.100$; $r(C^1H^3) = 1.085$; $r(C^2H^4) = 1.1202$; $r(O^2H^6) = 0.970$; $\sphericalangle C^1O^1C^2 = 120.3$; $\sphericalangle O^1C^2O^2 = 113.3$; $\sphericalangle H^1C^1O^1 = 108.9$; $\sphericalangle H^3C^1O^1 = 106.1$; $\sphericalangle H^1CH^2 = 106.8$; $\sphericalangle H^1CH^3 = 113.1$; $\sphericalangle O^1C^2H^4 = 105.2$; $\sphericalangle H^4C^2O^2 = 114.4$; $\sphericalangle C^2O^2H^6 = 112.7$; $\sphericalangle C^1O^1C^2O^2 = 0.0$; $\sphericalangle H^1C^1O^1C^2 = -57.9$; $\sphericalangle H^3C^1O^1C^2 = 180.0$; $\sphericalangle C^1O^1C^2H^4 = -125.7$; $\sphericalangle O^1C^2O^2H^6 = 180.0$.

9: C_s symmetry; $r(O^1O^2) = 1.469$; $r(C^1O^1) = 1.444$; $r(C^2O^2) = 1.239$; $r(C^1H^1) = 1.089$; $r(C^1H^3) = 1.095$; $r(C^2H^4) = 1.091$; $r(C^2H^5) = 1.092$; $\sphericalangle C^1O^1O^2 = 107.9$; $\sphericalangle O^1O^2C^2 = 112.7$; $\sphericalangle H^1C^1O^1 = 110.8$; $\sphericalangle H^2C^1O^1 = 100.1$; $\sphericalangle H^1C^1H^2 = 113.6$; $\sphericalangle H^3C^1H^1 = 110.4$; $\sphericalangle H^4C^2O^2 = 114.8$; $\sphericalangle H^5C^2O^2 = 120.6$; $\sphericalangle H^5C^2H^4 = 124.6$; $\sphericalangle C^1O^1O^2C^2 = 180.0$; $\sphericalangle H^4C^2O^2O^1 = 180.0$; $\sphericalangle H^5C^2O^2O^1 = 0.0$; $\sphericalangle O^2O^1C^1H^1 = -63.5$; $\sphericalangle O^2O^1C^1H^2 = 180.0$.

10: C_{2h} symmetry; $r(CO) = 1.246$; $r(CH^1) = 1.102$; $r(CH^2) = 1.106$; $r(OH^3) = 1.225$; $\sphericalangle H^1CO = 118.4$; $\sphericalangle H^2CO = 122.0$; $\sphericalangle H^1CH^2 = 119.6$; $\sphericalangle COH^3 = 118.3$; $\sphericalangle OH^3O = 180.0$; $\sphericalangle H^1COH^3 = 180.0$; $\sphericalangle H^2COH^3 = 0.0$.

11: C_s symmetry; $r(C^1O^1) = 1.229$; $r(C^2O^2) = 1.367$; $r(O^1H^3) = 1.192$; $r(O^2H^3) = 1.230$; $r(C^1H^1) = 1.093$; $r(C^1H^2) = 1.097$; $r(C^2H^4) = 1.090$; $r(C^2H^5) = 1.113$; $\sphericalangle H^1C^1O^1 = 121.6$; $\sphericalangle H^2C^1O^1 = 118.5$; $\sphericalangle H^1C^1H^2 = 119.9$; $\sphericalangle C^1O^1H^3 = 120.5$; $\sphericalangle O^1H^3O^2 = 179.6$; $\sphericalangle H^3O^2C^2 = 118.5$; $\sphericalangle O^2C^2H^4 = 115.2$; $\sphericalangle O^2C^2H^5 = 107.2$; $\sphericalangle H^4C^2H^5 = 100.0$; $\sphericalangle H^1C^1O^1H^3 = 180.0$; $\sphericalangle H^2C^1O^1H^3 = 0.0$; $\sphericalangle H^3C^2O^2H^4 = 0.0$; $\sphericalangle H^3O^2C^2H^5 = -126.8$.

0947-6539/97/0304-0636 $ 17.50+.50/0 Chem. Eur. J. 1997, 3, No. 4

12: C_1 symmetry; $r(C^1O^1)=1.208$; $r(C^2O^2)=1.437$; $r(O^1O^2)=2.232$; $r(C^1H^1)=1.101$; $r(C^1H^2)=1.104$; $r(C^2H^4)=1.099$; $r(C^2H^5)=1.093$; $r(C^2H^6)=1.086$; $r(O^2H^3)=0.974$; $\sphericalangle H^1C^1O^1=121.7$; $\sphericalangle H^2C^1O^1=118.9$; $\sphericalangle H^1C^1H^2=119.4$; $\sphericalangle C^1O^1O^2=108.3$; $\sphericalangle O^1O^2C^2=108.5$; $\sphericalangle O^1O^2H^3=92.2$; $\sphericalangle H^3O^2C^2=109.8$; $\sphericalangle O^2C^2H^4=107.2$; $\sphericalangle O^2C^2H^5=110.9$; $\sphericalangle O^2C^2H^6=107.2$; $\sphericalangle H^4C^2H^5=109.1$; $\sphericalangle H^4C^2H^6=110.0$; $\sphericalangle H^5C^2H^6=112.2$; $\sphericalangle H^1C^1O^1O^2=178.2$; $\sphericalangle H^2C^1O^1O^2=-1.8$; $\sphericalangle C^1O^1O^2C^2=-127.5$; $\sphericalangle C^1O^1O^2H^3=120.8$; $\sphericalangle H^3O^2C^2H^4=-68.1$; $\sphericalangle H^3O^2C^2H^5=50.9$; $\sphericalangle H^3O^2C^2H^6=173.8$.

13: C_1 symmetry; $r(C^1O^1)=1.516$; $r(C^2O^2)=1.210$; $r(O^1H^5)=1.048$; $r(O^2H^5)=1.516$; $r(C^1H^1)=1.095$; $r(C^1H^2)=1.096$; $r(C^1H^3)=1.094$; $r(O^1H^4)=0.985$; $r(C^2H^6)=1.122$; $\sphericalangle H^1C^1O^1=105.7$; $\sphericalangle H^2C^1O^1=109.2$; $\sphericalangle H^3C^1O^1=104.8$; $\sphericalangle H^1C^1H^2=112.8$; $\sphericalangle H^1C^1H^3=111.3$; $\sphericalangle H^2C^1H^3=112.5$; $\sphericalangle C^1O^1H^4=112.0$; $\sphericalangle C^1O^1H^5=113.5$; $\sphericalangle H^4O^1H^5=110.3$; $\sphericalangle O^1H^5O^2=177.0$; $\sphericalangle H^5O^2C^2=127.3$; $\sphericalangle O^2C^2H^6=123.9$; $\sphericalangle H^1C^1O^1H^4=-59.5$; $\sphericalangle H^1C^1O^1H^5=174.8$; $\sphericalangle H^2C^1O^1H^4=62.1$; $\sphericalangle H^2C^1O^1H^5=-63.6$; $\sphericalangle H^3C^1O^1H^4=-177.2$; $\sphericalangle H^3C^1O^1H^5=57.1$; $\sphericalangle H^4O^1H^5O^2=-123.4$; $\sphericalangle O^1H^5O^2C^2=-144.2$; $\sphericalangle H^5O^2C^2H^6=179.0$.

TS 1/11: C_s symmetry; $r(C^1O^1)=1.311$; $r(C^2O^2)=1.359$; $r(O^1O^2)=2.006$; $r(C^1H^1)=1.094$; $r(C^1H^3)=1.289$; $r(H^3O^1)=1.307$; $r(C^2H^4)=1.094$; $r(C^2H^5)=1.110$; $\sphericalangle H^1C^1O^1=119.0$; $\sphericalangle H^1C^1H^2=120.6$; $\sphericalangle H^3C^1O^1=60.3$; $\sphericalangle H^1C^1H^3=109.3$; $\sphericalangle C^1H^3O^1=60.7$; $\sphericalangle H^3O^1C^1=59.0$; $\sphericalangle C^1O^1O^2=112.1$; $\sphericalangle O^1O^2C^2=112.5$; $\sphericalangle H^4C^2O^2=114.2$; $\sphericalangle H^5C^2O^2=107.4$; $\sphericalangle H^4C^2H^5=111.8$; $\sphericalangle H^5C^2H^6=103.4$; $\sphericalangle H^1C^1O^1O^2=113.0$; $\sphericalangle H^3C^1O^1O^2=180.0$; $\sphericalangle C^1O^1O^2C^2=180.0$; $\sphericalangle O^1O^2C^2H^4=0.0$; $\sphericalangle O^1O^2C^2H^5=-125.0$.

TS 1/12: C_1 symmetry; $r(C^1O^1)=1.462$; $r(C^2O^2)=1.357$; $r(O^1O^2)=1.513$; $r(C^1H^1)=1.090$; $r(C^1H^2)=1.092$; $r(C^1H^3)=1.091$; $r(O^1H^4)=1.324$; $r(C^2H^4)=1.416$; $r(C^2H^5)=1.100$; $r(C^2H^6)=1.087$; $\sphericalangle H^1C^1O^1=110.5$; $\sphericalangle H^2C^1O^1=103.1$; $\sphericalangle H^3C^1O^1=106.1$; $\sphericalangle H^1C^1H^2=112.5$; $\sphericalangle H^1C^1H^3=111.4$; $\sphericalangle H^2C^1H^3=112.7$; $\sphericalangle C^1O^1O^2=113.4$; $\sphericalangle C^1O^1H^4=127.6$; $\sphericalangle H^4O^1O^2=79.8$; $\sphericalangle O^1O^2C^2=95.4$; $\sphericalangle O^2C^2H^4=82.3$; $\sphericalangle C^2H^4O^1=101.7$; $\sphericalangle H^5C^2O^2=116.1$; $\sphericalangle H^6C^2O^2=115.1$; $\sphericalangle H^5C^2H^6=120.0$; $\sphericalangle H^1C^1O^1O^2=-177.3$; $\sphericalangle H^2C^1O^1O^2=62.3$; $\sphericalangle H^3C^1O^1O^2=-60.1$; $\sphericalangle C^1O^1O^2C^2=-119.6$; $\sphericalangle C^1O^1H^4C^2=104.8$; $\sphericalangle H^4O^1O^2C^2=7.0$; $\sphericalangle O^1O^2C^2H^5=77.7$; $\sphericalangle O^1O^2C^2H^6=-134.6$.

TS 9/10: C_s symmetry; $r(C^1O^1)=1.309$; $r(C^2O^2)=1.212$; $r(O^1O^2)=2.007$; $r(C^1H^1)=1.094$; $r(C^1H^3)=1.280$; $r(H^3O^1)=1.328$; $r(C^2H^4)=1.100$; $\sphericalangle H^1C^1O^1=118.9$; $\sphericalangle H^1C^1H^2=120.5$; $\sphericalangle H^3C^1O^1=61.7$; $\sphericalangle H^1C^1H^3=109.1$; $\sphericalangle C^1H^3O^1=60.2$; $\sphericalangle H^3O^1C^1=58.1$; $\sphericalangle C^1O^1O^2=110.4$; $\sphericalangle O^1O^2C^2=114.0$; $\sphericalangle H^4C^2O^2=121.8$; $\sphericalangle H^5C^2O^2=119.2$; $\sphericalangle H^4C^2H^5=119.0$; $\sphericalangle H^1C^1O^1O^2=-82.9$; $\sphericalangle H^3C^1O^1O^2=180.0$; $\sphericalangle C^1O^1O^2C^2=180.0$; $\sphericalangle O^1O^2C^2H^4=0.0$; $\sphericalangle O^1O^2C^2H^5=180.0$.

TS 11/12: C_1 symmetry; $r(C^1O^1)=1.209$; $r(C^2O^2)=1.396$; $r(O^1O^2)=2.579$; $r(C^1H^1)=1.103$; $r(C^1H^2)=1.104$; $r(O^1H^3)=1.749$; $r(O^2H^3)=0.985$; $r(C^2H^4)=1.089$; $r(C^2H^5)=1.115$; $r(C^2H^6)=1.099$; $\sphericalangle H^1C^1O^1=121.8$; $\sphericalangle H^2C^1O^1=120.0$; $\sphericalangle H^1C^1H^2=118.2$; $\sphericalangle C^1O^1H^3=146.1$; $\sphericalangle O^1H^3O^2=139.5$; $\sphericalangle H^3O^2C^2=113.3$; $\sphericalangle O^2C^2H^4=113.7$; $\sphericalangle O^2C^2H^5=105.4$; $\sphericalangle O^2C^2H^6=108.3$; $\sphericalangle H^4C^2H^5=110.3$; $\sphericalangle H^4C^2H^6=114.5$; $\sphericalangle H^5C^2H^6=103.7$; $\sphericalangle H^1C^1O^1H^3=19.5$; $\sphericalangle H^2C^1O^1H^3=-160.5$; $\sphericalangle C^1O^1H^3O^2=-37.7$; $\sphericalangle O^1H^3O^2C^2=-101.5$; $\sphericalangle H^3O^2C^2H^4=5.9$; $\sphericalangle H^3O^2C^2H^5=-115.1$; $\sphericalangle H^3O^2C^2H^6=134.4$.

TS 12/4: C_1 symmetry; $r(C^1O^1)=1.238$; $r(C^2O^2)=1.350$; $r(O^1O^2)=2.658$; $r(C^1H^1)=1.105$; $r(C^1H^2)=1.110$; $r(C^1H^3)=1.538$; $r(C^2H^3)=1.216$; $r(C^2H^4)=1.090$; $r(C^2H^5)=1.093$; $r(O^2H^6)=0.968$; $\sphericalangle H^1C^1O^1=118.6$; $\sphericalangle H^2C^1O^1=116.6$; $\sphericalangle H^3C^1O^1=106.5$; $\sphericalangle H^1C^1H^2=117.2$; $\sphericalangle H^1C^1H^3=99.5$; $\sphericalangle H^2C^1H^3=91.1$; $\sphericalangle C^1O^1O^2=88.5$; $\sphericalangle O^1O^2C^2=87.6$; $\sphericalangle O^1O^2H^6=88.9$; $\sphericalangle H^6O^2C^2=113.1$; $\sphericalangle O^2C^2H^3=108.7$; $\sphericalangle O^2C^2H^4=111.4$; $\sphericalangle O^2C^2H^5=116.9$; $\sphericalangle H^3C^2H^4=101.4$; $\sphericalangle H^3C^2H^5=101.9$; $\sphericalangle H^4C^2H^5=114.6$; $\sphericalangle C^1H^3C^2=143.1$; $\sphericalangle H^1C^1O^1O^2=128.8$; $\sphericalangle H^2C^1O^1O^2=-82.0$; $\sphericalangle H^1C^1H^3C^2=-150.8$; $\sphericalangle H^2C^1H^3C^2=91.4$; $\sphericalangle C^1O^1C^2O^2=-20.8$; $\sphericalangle C^1O^1O^2H^6=-134.0$; $\sphericalangle O^1O^2C^2H^3=8.0$; $\sphericalangle O^1O^2C^2H^4=118.9$; $\sphericalangle O^1O^2C^2H^5=-106.7$; $\sphericalangle O^2C^2H^3C^1=4.8$.

TS 13-H_2: C_1 symmetry; $r(CO)=1.445$; $r(CH^1)=1.089$; $r(CH^2)=1.089$; $r(OH^3)=0.973$; $r(CH^4)=1.238$; $r(OH^5)=1.451$; $r(H^4H^5)=0.973$; $\sphericalangle H^1CO=110.8$; $\sphericalangle H^2CO=116.4$; $\sphericalangle H^4CO=109.7$; $\sphericalangle H^1CH^2=116.6$; $\sphericalangle H^1CH^4=100.8$; $\sphericalangle H^2CH^4=100.6$; $\sphericalangle COH^3=111.1$; $\sphericalangle COH^5=54.2$; $\sphericalangle H^3OH^5=113.5$; $\sphericalangle OH^5H^4=128.9$; $\sphericalangle H^5H^4C=69.2$; $\sphericalangle H^1COH^3=-143.6$; $\sphericalangle H^2COH^3=-7.2$; $\sphericalangle H^4COH^3=106.0$; $\sphericalangle H^5H^4CO=-2.7$; $\sphericalangle H^5H^4CH^1=-119.6$; $\sphericalangle H^5H^4CH^2=120.5$.

Acknowledgment. We are indebted to Prof. Johan K. Terlouw for helpful discussions and comments. Further, we thank Martin Dieterle for assistance in performing the calculations. Continuous financial support by the Deutsche Forschungsgemeinschaft, the Volkswagen-Stiftung, and the Fonds der Chemischen Industrie is gratefully acknowledged.

Received: October 23, 1996 [F 506]

[1] a) L. Radom, *Org. Mass Spectrom.* **1991**, *26*, 359; b) R. Zahradník, *Acc. Chem. Res.* **1995**, *28*, 306.

[2] See, for example: a) P. C. Burgers, J. L. Holmes, C. E. C. A. Hop, R. Postma, P. J. A. Ruttink, J. K. Terlouw, *J. Am. Chem. Soc.* **1987**, *109*, 7315; b) B. F. Yates, W. J. Bouma, J. K. MacLeod, L. Radom, *J. Chem. Soc. Chem. Commun.* **1987**, 204; c) J. R. Cao, M. George, J. L. Holmes, M. Sirois, J. K. Terlouw, P. C. Burgers, *J. Am. Chem. Soc.* **1992**, *114*, 2017; d) H. E. Audier, A. Milliet, D. Leblanc, T. H. Morton, *J. Am. Chem. Soc.* **1992**, *114*, 2020; e) P. J. A. Ruttink, P. C. Burgers, *Org. Mass Spectrom.* **1993**, *28*, 1087; f) D. Suh, P. C. Burgers, J. K. Terlouw, *Rap. Commun. Mass Spectrom.* **1995**, *9*, 862.

[3] For reviews dealing with ion/dipole complexes, see: a) T. H. Morton, *Tetrahedron* **1982**, *38*, 3195; b) N. Heinrich, H. Schwarz in *Ion and Cluster Ion Spectroscopy*, (Ed.: J. P. Maier), Elsevier, Amsterdam, **1989**, p. 328; c) R. D. Bowen, *Acc. Chem. Res.* **1991**, *24*, 364; d) P. Longevialle, *Mass Spectrom. Rev.* **1992**, *11*, 157.

[4] a) D. J. Bellvile, R. A. Pabon, N. L. Bauld, *J. Am. Chem. Soc.* **1985**, *107*, 4978; b) B. F. Yates, W. J. Bouma, L. Radom, *Tetrahedron* **1986**, *42*, 6234.

[5] For reviews, see: a) L. S. Silbert in *Organic Peroxides*, Vol. II (Ed.: D. Swern), Wiley, New York, **1971**, p. 730; b) H. Schwarz, H.-M. Schiebel in *The Chemistry of Peroxides* (Ed.: S. Patai), Wiley, New York, **1983**, p. 105; c) W. A. König in: Houben-Weyl, *Methoden der organischen Chemie*, Vol. E13/2, Thieme, Stuttgart, **1988**, p. 1466.

[6] R. T. M. Fraser, N. C. Paul, L. Philips, *J. Chem. Soc. (B)* **1970**, 1278.

[7] J. H. van Driel, W. Heerma, J. K. Terlouw, H. Halim, H. Schwarz, *Org. Mass Spectrom.* **1985**, *20*, 665.

[8] D. Schröder, D. Sülzle, O. Dutuit, T. Baer, H. Schwarz, *J. Am. Chem. Soc.* **1994**, *116*, 6395, and references therein.

[9] a) R. Srinivas, D. Sülzle, T. Weiske, H. Schwarz, *Int. J. Mass Spectrom. Ion Processes* **1991**, *107*, 368; b) R. Srinivas, D. Sülzle, W. Koch, C. H. DePuy, H. Schwarz, *J. Am. Chem. Soc.* **1991**, *113*, 5970; c) C. A. Schalley, D. Schröder, H. Schwarz, *Int. J. Mass Spectrom. Ion Processes*, **1996**, *153*, 173.

[10] C. A. Schalley, R. Wesendrup, D. Schröder, H. Schwarz, *J. Am. Chem. Soc.* **1994**, *116*, 11089.

[11] K. L. Busch, G. L. Glish, S. A. McLuckey, *Mass Spectrometry/Mass Spectrometry: Techniques and Applications of Tandem Mass Spectrometry*, VCH, Weinheim **1988**.

[12] P. Scheier, T. D. Märk, *Int. J. Mass Spectrom. Ion Processes* **1992**, *113*, R 7.

[13] A. A. Mommers Ph.D. Thesis, University of Utrecht, The Netherlands, **1985**.

[14] For reviews dealing with NR techniques, see: a) C. Wesdemiotis, F. W. McLafferty, *Chem. Rev.* **1987**, *87*, 485; b) J. K. Terlouw, H. Schwarz, *Angew. Chem. Int. Ed. Engl.* **1987**, *26*, 805; c) J. L. Holmes, *Mass Spectrom. Rev.* **1989**, *8*, 513; d) A. W. McMahon, S. K. Chowdhury, A. G. Harrison, *Org. Mass Spectrom.* **1989**, *24*, 620; e) F. W. McLafferty, *Science* **1990**, *247*, 925; f) N. Goldberg, H. Schwarz, *Acc. Chem. Res.* **1994**, *27*, 347.

[15] Following the terminology proposed in ref. [14d] $^+NR^-$ means that a beam of cations is neutralized and reionized to anions, while $^+NR^+$ describes the more common NR procedure in which projectile as well as product ions are positively charged.

[16] See, for example: a) P. C. Burgers, J. L. Holmes, A. A. Mommers, J. E. Szulejko, J. K. Terlouw, *Org. Mass Spectrom.* **1984**, *19*, 442; b) J. L. Holmes, A. A. Mommers, *Org. Mass Spectrom.* **1984**, *19*, 460.

[17] We use a terminology in analogy to that proposed for the NR experiments, e.g., $^+CR^-$ means that cations were collided with a collision gas to produce anions.

[18] a) R. G. Cooks, J. H. Beynon, R. M. Caprioli, G. R. Lester, *Metastable Ions*, Elsevier, Amsterdam, 1973; b) J. L. Holmes, J. K. Terlouw, *Org. Mass Spectrom.* **1980**, *15*, 383.

[19] a) K. Eller, H. Schwarz, *Int. J. Mass Spectrom. Ion Processes* **1989**, *93*, 243; b) K. Eller, W. Zummack, H. Schwarz, *J. Am. Chem. Soc.* **1990**, *112*, 621.

[20] R. A. Forbes, F. H. Laukien, J. Wronka, *Int. J. Mass Spectrom. Ion Processes* **1988**, *83*, 23.

[21] A. Rieche, W. Brumshagen, *Chem. Ber.* **1928**, *61*, 951.

[22] A. Rieche, F. Hitz, *Chem. Ber.* **1929**, *62*, 2458.

[23] C. Walling, S. A. Buckler, *J. Am. Chem. Soc.* **1953**, *75*, 4372.

[24] A. F. Kluge, K. G. Untch, J. H. Fried, *J. Am. Chem. Soc.* **1972**, *94*, 7827.

[25] $HOCH_2OCH_3$, **4**, is not stable in the condensed phase; rather it undergoes both acid- and base-catalyzed dissociation into methanol and formaldehyde with the equilibrium far on the side of the dissociated molecules. Therefore, the synthesis of appropriate precursors would be necessary, which, upon dissociative ionization, would give rise to the corresponding radical cations in the ion source. However, all attempts failed to generate ions, which unequivocally have the $HOCH_2OCH_3^{\cdot+}$ connectivity.

[26] L. Caglioti, F. Gasparrini, D. Misiti, G. Palmieri, *Tetrahedron* **1978**, *34*, 135.

[27] E. S. Shanley in *Organic Peroxides*, Vol. 3 (Ed.: D. Swern), Wiley: New York, **1972**, p. 341.

[28] GAUSSIAN 94, Revision B3: M. J. Frisch, G. W. Trucks, H. W. Schlegel, P. M. W. Gill, B. G. Johnson, M. A. Robb, J. R. Cheeseman, T. Keith, G. A. Peterson, J. A. Montgomery, K. Raghavachari, M. A. Al-Laham, V. G. Zakrzewski, J. V. Ortiz, J. B. Foresman, C. Y. Peng, P. Y. Ayala, W. Chen, M. W. Wong, J. L. Andres, E. S. Replogle, R. Gomperts, R. L. Martin, D. J. Fox, J. S. Binkley, D. J. Defrees, J. Baker, J. P. Stewart, M. Head-Gordon, C. Gonzales, J. A. Pople, GAUSSIAN, Pittsburgh PA, **1992**.

[29] a) L. A. Curtiss, K. Raghavachari, G. W. Trucks, J. A. Pople, *J. Chem. Phys.* **1991**, *94*, 7221; b) L. A. Curtiss, K. Raghavachari, J. A. Pople, *J. Chem. Phys.* **1993**, *98*, 1293; c) For a modification of the G2 approach using DFT, see: C. W. Bauschlicher, Jr., H. Partridge, *J. Chem. Phys.* **1995**, *103*, 1788.
[30] R. Kishnan, J. S. Binkley, R. Seeger, J. A. Pople, *J. Chem. Phys.* **1980**, *72*, 650.
[31] a) G. Rauhut, R. Pulay, *J. Phys. Chem.* **1995**, *99*, 3093; b) A. P. Scott, L. Radom, *ibid.* **1996**, *100*, 16502.
[32] P. M. W. Gill, B. G. Johnson, J. A. Pople, *Chem. Phys. Lett.* **1992**, *197*, 499.
[33] For example, see: J. Hrušák, H. Friedrichs, H. Schwarz, H. Razafinjanahary, H. Chermette, *J. Phys. Chem.* **1996**, *100*, 100.
[34] C. A. Schalley, J. Harvey, D. Schröder, H. Schwarz, unpublished result.
[35] K. Fukui, *Acc. Chem. Res.* **1981**, *14*, 363.
[36] a) C. Gonzalez, H. B. Schlegel, *J. Chem. Phys.* **1989**, *90*, 2154; b) C. Gonzalez, H. B. Schlegel, *J. Phys. Chem.* **1990**, *94*, 5523.
[37] a) P. Fournier, J. Appell, F. C. Fehsenfeld, J. Durup, *J. Phys.* **1972**, *B5*, L58; b) F. C. Fehsenfeld, J. Appell, P. Fournier, J. Durup, *J. Phys.* **1973**, *B6*, L268; c) J. C. Lorquet, B. Leyh-Nihaut, F. W. McLafferty, *Int. J. Mass Spectrom. Ion Processes* **1990**, *100*, 465.
[38] a) D. M. Hudgins, R. F. Porter, *Int. J. Mass Spectrom. Ion Processes* **1994**, *130*, 49; b) M. Iraqi, N. Goldberg, H. Schwarz, *ibid.* **1994**, *130*, 127.
[39] For a review on distonic ions, see: a) S. Hammerun, *Mass Spectrom. Rev.* **1988**, *7*, 123; b) K. M. Stirk, L. K. Kiminkinen, H. I. Kenttämaa, *Chem. Rev.* **1992**, *92*, 1649. For the relative thermodynamic stabilities and kinetic barriers of $CH_3OH^{\bullet +}$ versus $^{\bullet}CH_2OH_2^+$ and the corresponding neutrals as a model for $CH_3OO^+(H)CH_2^{\bullet}$, see: c) W. J. Bouma, J. K. MacLeod, L. Radom, *J. Am. Chem. Soc.* **1982**, *104*, 2930; d) J. L. Holmes, F. P. Lossing, J. K. Terlouw, P. C. Burgers, *ibid.* **1982**, *104*, 2931; e) H. Schwarz, *Nachr. Chem. Tech. Lab.* **1983**, *31*, 451; f) L. Radom, W. J. Bouma, R. H. Nobes, B. F. Yates, *Pure Appl. Chem.* **1984**, *56*, 1831; g) See also: H. E. Audier, D. Leblanc, P. Mourgues, T. B. McMahon, S. Hammerum, *J. Chem. Soc. Chem. Commun.* **1994**, 2329.
[40] In addition, all attempts to characterize a $CH_3OO^+(H)CH_2^{\bullet}$ distonic ion by ab initio calculations failed.
[41] The similarity between CA and NR/CA mass spectra has been interpreted as being indicative for a structurally "pure" ion beam formed in the ion source, see: P. C. Burgers, G. A. McGibbon, J. K. Terlouw, *Chem. Phys. Lett.* **1994**, *224*, 539.
[42] a) G. Hvistendahl, E. Uggerud, *Org. Mass Spectrom.* **1991**, *26*, 67; b) E. Uggerud, T. Helgaker, *J. Am. Chem. Soc.* **1992**, *114*, 4265.
[43] a) R. A. Bair, W. A. Goddard III, *J. Am. Chem. Soc.* **1982**, *104*, 2719; b) W. Gase, J. E. Boggs, *J. Mol. Struct.* **1984**, *116*, 207; c) D. Christen, H.-D. Mack, H. Oberhammer, *Tetrahedron* **1988**, *44*, 7363. d) M.-B. Huang, H. U. Suter, *J. Mol. Struct.* **1994**, *337*, 173.
[44] K. Kimura, K. Osafune, *Bull. Chem. Soc. Jpn.* **1975**, *48*, 2421.
[45] a) P. Rademacher, W. Elling, *Liebigs Ann. Chem.* **1979**, 1473; b) B. Haas, H. Oberhammer, *J. Am. Chem. Soc.* **1984**, *106*, 6146.
[46] C. Glidewell, *J. Mol. Struct.* **1980**, *67*, 35.
[47] J. W. Larson, T. B. McMahon, *J. Am. Chem. Soc.* **1982**, *104*, 6255.
[48] Unless stated otherwise, thermochemical data are taken from: a) G. Lias, J. E. Bartmess, J. F. Liebman, J. L. Holmes, R. D. Levin, W. G. Mallard, *J. Phys. Chem. Ref. Data, Suppl. 1* **1988**; b) S. G. Lias, J. F. Liebman, R. D. Levin, S. A. Kafafi, *NIST Standard Reference Database, Positive Ion Energetics*, Version 2.01, Gaithersburg, MD, **1994**.
[49] P. C. Burgers, J. L. Holmes, *Org. Mass Spectrom.* **1984**, *19*, 452.
[50] The origin of the increased BDE of the peroxidic O–O bond in $\mathbf{1}^{\bullet +}$ has been discussed previously, see: E. E. Ferguson, J. Roncin, L. Bonazzola, *Int. J. Mass Spectrom. Ion Processes* **1987**, *79*, 215.
[51] For an ab initio calculation on the heat of formation and the ionization energy of $CH_3OO^{\bullet}$, see: Y.-S. Cheung, W.-K. Li *Chem. Phys. Lett.* **1994**, *223*, 383.
[52] The C–H bond strength of neutral **1** is estimated on the basis of data for methanol as a model compound (ref. [48]).
[53] Some examples for large primary KIE values in the unimolecular decay of small organic cations have been reported earlier: a) see ref. [8]; b) R. D. Bowen, D. H. Williams, H. Schwarz, *Angew. Chem. Int. Ed. Engl.* **1979**, *18*, 451.
[54] a) S. A. McLuckey, D. Cameron, R. G. Cooks, *J. Am. Chem. Soc.* **1981**, *103*, 1313; b) R. G. Cooks, J. S. Patrick, T. Kotiaho, S. A. McLuckey, *Mass Spectrom. Rev.* **1995**, *13*, 287.
[55] The intensity differences between the MI/CA spectrum of $[\mathbf{1} - H]^+$ and the reference CA spectrum of the proton-bound dimer of formaldehyde are probably due to differences in the internal energy content, which result from the different ionization methods (i.e. EI vs. CI).
[56] C. A. Schalley, D. Schröder, H. Schwarz, *Helv. Chim. Acta*, **1995**, *78*, 1999.
[57] For thermochemical data of the methoxy cation and the barrier for the decomposition reaction $CH_3O^+ \rightarrow HCO^+ + H_2$, see for example: a) K. Hiraoka, P. Kebarle, *J. Am. Chem. Soc.* **1977**, *99*, 366; b) B. Ruscic, J. Berkowitz, *J. Chem. Phys.* **1991**, *95*, 4033; c) L. A. Curtiss, L. D. Kock, *ibid.* **1991**, *95*, 4040; d) D. R. Yarkony, *J. Am. Chem. Soc.* **1992**, *114*, 5406.
[58] a) M. J. S. Dewar, H. S. Rzepa, *J. Am. Chem. Soc.* **1977**, *99*, 7432; b) W. J. Bouma, R. H. Nobes, L. Radom, *Org. Mass Spectrom.* **1982**, *17*, 315.
[59] The reaction of unlabeled reactants has also been carried out in a SIFT mass spectrometer, see: N. G. Adams, D. Smith, D. Grief, *Int. J. Mass Spectrom. Ion Phys.* **1978**, *26*, 405.
[60] a) P. J. A. Ruttink in *The Structure of Small Radicals and Ions* (Eds.: R. Naaman, Z. Vager), Plenum Press, New York, **1981**, p. 243; b) G. Schaftenaar, R. Postma, P. J. A. Ruttink, P. C. Burgers, G. A. McGibbon, J. K. Terlouw, *Int. J. Mass Spectrom. Ion Processes*, **1990**, *100*, 521.
[61] N. Heinrich, J. Schmidt, H. Schwarz, Y. Apeloig, *J. Am. Chem. Soc.* **1987**, *109*, 1317.

0947-6539/97/0304-0638 $ 17.50+.50/0 *Chem. Eur. J.* **1997**, *3*, *No. 4*